



Effect of Anisotropic Parameters on Flow Structure and Heat Transfer in a Channel Partially Filled with an Anisotropic Porous Layer



Salah Ben Aoua¹, Rachid Kibboua², Farid Mechighel^{1*}

¹ Mechanics of Materials and Industrial Maintenance Research Laboratory (LR3MI), Mechanical Engineering Department, Faculty of Technology, Badji Mokhtar – Annaba University, 23000 Annaba, Algeria

² Faculty of Mechanical Engineering and Process Engineering, University of Sciences and Technologies Houari Boumediene (USTHB), Laboratory of Multiphase Transport and Porous Media (LTPMP), 16111 Algiers, Algeria

* Correspondence: Farid Mechighel (farid.mechighel@univ-annaba.dz)

Received: 03-19-2026

Revised: 05-15-2026

Accepted: 05-25-2026

Citation: S. Ben Aoua, R. Kibboua, and F. Mechighel, “Effect of anisotropic parameters on flow structure and heat transfer in a channel partially filled with an anisotropic porous layer,” *Power Eng. Eng. Thermophys.*, vol. 5, no. 2, pp. 140–162, 2026. <https://doi.org/10.56578/peet050205>.



© 2026 by the author(s). Licensee Acadlore Publishing Services Limited, Hong Kong. This article can be downloaded for free, and reused and quoted with a citation of the original published version, under the CC BY 4.0 license.

Abstract: This study examines the effect of inserting an anisotropic porous layer on flow and heat transfer in a channel partially filled by this layer. The main objective of this study is to evaluate the influence of the porous layer’s anisotropy parameters, specifically: the anisotropic permeability ratio and the anisotropy orientation angle, as well as the permeability (related to the Darcy number Da) and thickness of the porous layer. Other parameters affecting flow and heat transfer, such as the Forchheimer inertia coefficient (Forchheimer drag coefficient) and the ratio of the thermal conductivities of the porous layer and the fluid, are also considered. The results, expressed in terms of velocity profiles, temperature profiles, Nusselt number, friction coefficient, and overall thermohydraulic performance, reveal several significant physical trends. The influence of the Forchheimer inertia coefficient on the Nusselt number becomes negligible when Da is low ($Da \ll 1$), a regime where viscous effects dominate and attenuate the contribution of inertial forces to momentum transport. Conversely, the anisotropic permeability ratio and the anisotropy orientation angle in the porous layer strongly affect the flow structure and thermal response by altering the preferred direction of transport within this layer. The thickness of this layer induces an explicit compromise between improving heat transfer and increasing hydraulic resistance. Indeed, an intermediate thickness allows increasing the Nusselt number without disproportionately increasing pressure drops. Furthermore, in partially filled configurations, an effective thermal conductivity of the porous layer lower than that of the solid wall tends to concentrate the thermal gradient at the interface fluid/porous layer, which can locally intensify heat transfer compared to the case of a fully filled channel. Taken together, these results demonstrate how permeability, structural anisotropy parameters (anisotropic permeability ratio and anisotropy orientation angle), and porous layer thickness jointly control the thermal and hydraulic performance of the channel, and provide useful selection criteria for the design of partially porous channel thermal systems, in which intensifying heat transfer and minimizing pressure drop are competing objectives that must be achieved simultaneously.

Keywords: Anisotropic parameters; Porous layer; Partially porous channel; Thermohydraulic performance; Flow and heat transfer

1 Introduction

In recent years, considerable research efforts have been devoted to the study of heat transfer phenomena by natural and/or forced convection in channels filled with fluid-saturated porous media. This research has numerous applications in modern thermal system technologies, including the design of compact heat exchangers, solar collectors, geothermal converters, building insulation materials, electronic coolers, and catalytic converters. Other practical examples include the modeling of geophysical flows, oil reservoirs, and subsurface pollutant diffusion, among others [1–6].

Techniques aimed at improving heat transfer in thermal systems generally fall into two categories: passive and active methods. Passive methods, which do not require an external power supply, include, for example, the use of fins, the addition of additives to the fluid, and the incorporation of porous media into the system, as discussed in

this article [7–12]. In contrast, active methods require an external energy source, such as surface vibrations or the application of electric or magnetic fields [13, 14].

Research on convective heat transfer in fluid-saturated porous media primarily focuses on isotropic materials [2]. Studies examine fluid flow in channels partially filled with isotropic porous materials. For instance, Kuznetsov [15] provided analytical solutions for fully developed laminar flow in such channels using the Darcy-Brinkman-Forchheimer model, showing that shear stress jumps significantly affect the velocity profile. In another study, Kuznetsov [16] generalized Darcy's law to include viscous effects at pore boundaries, analyzing the impact of the Darcy number on velocity in partially filled channels. He also explored forced convection in parallel-plate channels with homogeneous porous materials [17], using the Darcy-Brinkman-Forchheimer equation to analyze velocity and temperature distributions. Kuznetsov [18] investigated forced convection from a flat plate with an isotropic porous substrate, predicting velocity and temperature distributions under uniform heat flux conditions. Cekmer et al. [19] analyzed forced convection in flat channels with porous matrices, finding that the heat transfer enhancement ratio (ε_T) was significantly influenced by the Darcy number, but not by the ratio of thermal conductivities (R_k^*) when $R_k^* \geq 0.2$. Maerefat et al. [20] conducted a numerical study on porous materials in circular pipes, finding that increasing porous thickness generally increased the Nusselt number in core configurations, while it decreased in annular configurations with low thermal conductivity.

All of these this research studies emphasize the role of isotropic porous materials in enhancing heat transfer and highlights the importance of material properties in optimizing performance. Future studies could refine these findings to improve thermal management in porous media applications.

Nevertheless, in many applications, porous media exhibit anisotropic mechanical and thermal properties, often due to preferential orientation or asymmetric geometry of grains or fibers [21]. The first study of convective heat transfer in an anisotropic porous medium was conducted by the research [22], assuming that the porous layer was saturated by a fluid between two horizontal or inclined plates at constant temperature. Linear stability analysis determined the natural convection threshold.

Other research has examined forced or mixed convection in saturated anisotropic porous media. Degan and Vasseur [23] analyzed mixed convection in an anisotropic porous channel between two vertical walls at constant temperature. They found that at low Darcy numbers (indicating low porosity), the velocity distribution and heat transfer resemble pure Darcy behavior (valid for $Da \geq 10^{-5}$), with negligible viscosity effects near walls. However, at high Da values (indicating high porosity), the orientation of the anisotropic permeability ratio (K^*) significantly affects heat transfer. At very high Da ($Da \geq 10$), frictional resistance increases, diminishing anisotropic effects and converging results toward those of a pure fluid. Nakayama et al. [24] conducted a pore-scale numerical study simulating fluid flow and heat transfer in anisotropic porous media, proposing a model with square rods to represent the microscopic structure. Their results indicated that the directional interfacial heat transfer coefficient varies similarly to directional permeability based on the macroscopic flow angle. Degan et al. [21] provided an analytical solution for forced convection in an anisotropic permeable horizontal channel, using Brinkman's extended Darcy model under no-slip conditions. Their findings revealed that anisotropic parameters (K^* and θ) significantly influence fluid flow and heat transfer, particularly at low porosity ($Da \leq 10^{-4}$). Heat transfer is maximized when the principal axis of highest permeability aligns with the gravity vector and minimized when perpendicular.

Finally, other research has focused on forced convection in fluid-saturated anisotropic porous channels. Among these studies, the impact of hydrodynamic dispersion on convection in an anisotropic porous medium has been particularly important [25]. In addition, research has been conducted on double diffusion-convection in these media [26, 27]. General studies on forced or natural convection in channels filled with fluid-saturated porous media are also available [28, 29].

To the best of the authors' knowledge, a review of the literature on this topic reveals several important points. First, the majority of studies on forced convection in channels filled with fluid-saturated porous media have assumed an isotropic medium. Second, among the research on anisotropic media, most have focused on the effects of anisotropic permeability ratio and anisotropy orientation angle, neglecting other parameters influencing hydrodynamic anisotropy. In particular, variations in the porous layer thickness (E^*) and anisotropic permeability tensor [\mathbf{K}], as well as the Da , have often been omitted. Most studies have been conducted in partially filled channels with fixed values for these parameters, especially the layer thickness. Furthermore, the impact of the ratio of thermal conductivities (between the porous medium and the fluid, $R_k^* = k_{\text{eff}}/k_f$) and the Forchheimer inertia coefficient number (F) was considered negligible.

All of these parameters can significantly influence heat transfer and flow in the porous medium. Therefore, the results of these studies may be incomplete. It is essential to include all of these parameters to obtain more accurate results during numerical simulations.

Considering these parameters is important for assessing heat transfer enhancement. Although the addition of a porous medium improves heat transfer, this is accompanied by an increase in pressure drops, highlighting the importance of thickness on heat transfer and flow. Therefore, it is necessary to find a compromise between

improving heat transfer and controlling pressure drops by determining the optimal thickness and the ideal anisotropic hydrodynamic properties of the layer.

The main objectives of this study are to highlight the effects of anisotropic parameters on heat transfer and flow in a channel partially filled with an anisotropic layer. This research also aims to explore how to improve heat transfer by combining different anisotropic hydrodynamic parameters (Da , θ and E^*) to clarify the trade-off between heat transfer and pressure losses. Finally, this study addresses a growing need for research on the impact of anisotropic hydrodynamic parameters in channel systems partially filled with porous media.

2 General Considerations and Mathematical Model

2.1 Presentation of the Physical Problem

Consider the physical problem illustrated in Figure 1. The domain is a channel with two horizontal planar surfaces of length l and separated by a distance $2H$, partially filled with an anisotropic porous layer saturated with fluid. Since the channel length is much greater than its width, a two-dimensional (2D) flow approach is appropriate.

The anisotropic porous layer consists of two identical parts of thickness e_p , positioned between the bottom and top surfaces of the channel. A constant heat flux per unit area q_w is applied to both surfaces. The Ox' axis aligns with the bottom wall (see Figure 1). Due to the symmetry of the system, only the lower part is analyzed, with the central axis of the channel serving as the axis of symmetry.

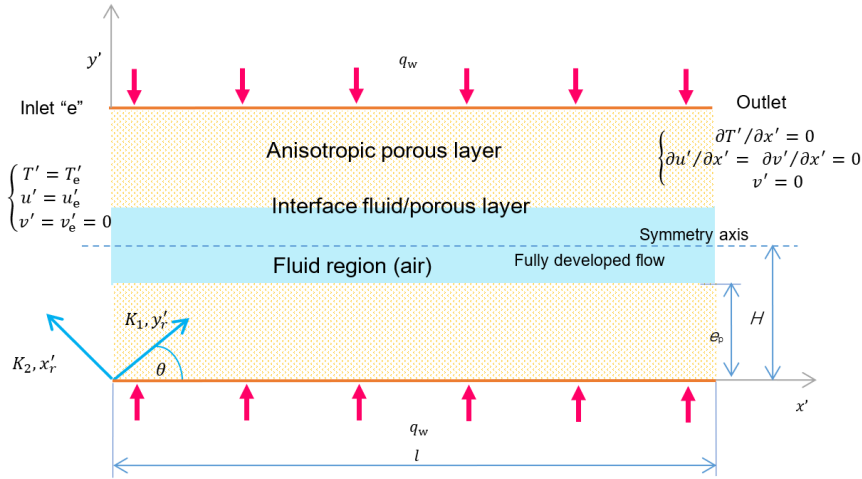


Figure 1. Typical configuration of a partially filled channel with an anisotropic porous layer saturated with a fluid
Note: u'_e , v'_e , and T'_e represent the velocities and temperature at the channel inlet, respectively. Other terms used in the figure are presented later.

2.1.1 Assumptions

In this study, the following assumptions are adopted: The porous medium is considered anisotropic, with anisotropic permeability and isotropic thermal conductivity. The permeability components along the two principal axes are denoted K_1 and K_2 , and the permeability anisotropy ratio is defined as $K^* = K_1/K_2$. The angle between the horizontal direction Ox' and the principal permeability axis K_2 is designated as the anisotropy orientation angle θ (Figure 1).

For the fluid region, the 2D forced flow is assumed to be laminar, with the fluid being viscous, Newtonian, and incompressible. Volumetric forces, such as gravitational force, are neglected, making the thermal effects related to temperature variation insignificant under the Boussinesq approximation, thus justifying a constant heat flux.

Furthermore, radiation and viscous dissipation are neglected, and there are no internal heat sources in the model. Natural convection interactions are ignored, as previous studies, including Aicher and Martin [30], indicate that these effects have minimal impact on heat transfer coefficients compared to forced convection.

Finally, we assume that: (i) the flow in both the channel and the porous medium is fully developed, (ii) the fluid is in local thermal equilibrium with the porous layer, and (iii) the thermophysical properties of the fluid and the anisotropic hydrodynamic parameters of the porous layer remain constant. Accurate modeling of anisotropic media necessitates the integration of realistic matrix properties.

2.2 Governing Equations

To formulate the equations governing the flow of fluid in the channel filled with a porous medium (Figure 1), it is necessary to use the Navier-Stokes equations in the fluid region and the nonlinear Darcy-Brinkman-Forchheimer equation in the porous region.

2.2.1 Fluid region

$$\vec{\nabla} \cdot \vec{V}' = 0 \quad (1)$$

where, \vec{V}' denotes the fluid velocity; $\vec{\nabla}$ denotes the vector differential del operator. Note that the prime superscript denotes dimensional quantities: for example, the velocity components (u' , v') in m/s, the pressure p' in Pa, and the temperature T' in K.

$$\rho_f \left(\partial \vec{V}' / \partial t + \vec{V}' \cdot \vec{\nabla} \vec{V}' \right) = -\vec{\nabla} p' + \mu_f \nabla^2 \vec{V}' \quad (2)$$

where, ρ_f and μ_f denote the fluid density and dynamic viscosity, respectively.

Assuming steady flow, the projections of the momentum equation in Cartesian coordinates are as follows:

In the horizontal direction (designated as axial, x'), which aligns with the axis of symmetry of the channel, and in the vertical direction (referred to as transverse, y'), the equations are respectively:

$$\rho_f \left(u' \frac{\partial u'}{\partial x'} + v' \frac{\partial u'}{\partial y'} \right) = -\frac{\partial p'}{\partial x'} + \mu_f \left(\frac{\partial^2 u'}{\partial x'^2} + \frac{\partial^2 u'}{\partial y'^2} \right) \quad (3)$$

$$\rho_f \left(u' \frac{\partial v'}{\partial x'} + v' \frac{\partial v'}{\partial y'} \right) = -\frac{\partial p'}{\partial y'} + \mu_f \left(\frac{\partial^2 v'}{\partial x'^2} + \frac{\partial^2 v'}{\partial y'^2} \right) \quad (4)$$

2.2.2 Anisotropic porous region

$$\rho_f \left[\frac{\partial \vec{V}'_r}{\varepsilon \partial t} + \frac{1}{\varepsilon^2} \vec{V}'_r \cdot \vec{\nabla} \vec{V}'_r \right] = -\vec{\nabla} p'_r + \rho_f \vec{F}_v + \mu_{\text{eff}} \nabla^2 \vec{V}'_r - \mu_f [K]^{-1} \vec{V}'_r - \rho_f F \sqrt{[K]^{-1}} \left| \vec{V}'_r \right| \vec{V}'_r \quad (5)$$

where, $\left| \vec{V}'_r \right| = \sqrt{u_r'^2 + v_r'^2}$ represents the superficial velocity of the flow along the principal axes of the anisotropic porous layer (x'_r , y'_r) (Figure 1). \vec{F}_v refers to volume force, μ_{eff} denotes the effective thermal conductivity of the porous layer, and ε its porosity, and F represents the Forchheimer inertia coefficient (Forchheimer drag coefficient). The subscript “ r ” is used to represent the rotation matrices relating the velocity components in the two coordinate systems (x'_r , y'_r) and (x' , y'). The permeability tensor of the anisotropic porous medium, which is a non-zero positive quantity, can be expressed as:

$$\sqrt{[K]^{-1}} = \begin{bmatrix} 1/\sqrt{K_2} & 0 \\ 0 & 1/\sqrt{K_1} \end{bmatrix} \quad (6)$$

The momentum equation (Eq. (5)) can be written as follows:

$$\frac{\rho_f}{\varepsilon^2} \begin{pmatrix} u'_r \frac{\partial u'_r}{\partial x'_r} + v'_r \frac{\partial u'_r}{\partial y'_r} \\ u'_r \frac{\partial v'_r}{\partial x'_r} + v'_r \frac{\partial v'_r}{\partial y'_r} \end{pmatrix} = \begin{pmatrix} -\frac{\partial p'_r}{\partial x'_r} \\ -\frac{\partial p'_r}{\partial y'_r} \end{pmatrix} + \mu_{\text{eff}} \begin{pmatrix} u'_r \frac{\partial^2 u'_r}{\partial x_r'^2} + v'_r \frac{\partial^2 u'_r}{\partial y_r'^2} \\ u'_r \frac{\partial^2 v'_r}{\partial x_r'^2} + v'_r \frac{\partial^2 v'_r}{\partial y_r'^2} \end{pmatrix} - \mu_f [K]^{-1} \begin{pmatrix} u'_r \\ v'_r \end{pmatrix} - \rho_f F \sqrt{[K]^{-1}} \sqrt{u_r'^2 + v_r'^2} \begin{pmatrix} u'_r \\ v'_r \end{pmatrix} \quad (7)$$

Eq. (7) can be reformulated in the main axes of the system (x' , y') using rotation matrices to connect the velocity components between coordinate systems (x'_r , y'_r) and (x' , y') (Eq. (8)). The inverse of this matrix is given by (Eq. (9)).

$$\begin{pmatrix} u'_r \\ v'_r \end{pmatrix} = \begin{bmatrix} +\cos \theta & \sin \theta \\ -\sin \theta & \cos \theta \end{bmatrix} \begin{pmatrix} u' \\ v' \end{pmatrix} \quad (8)$$

$$\begin{pmatrix} u' \\ v' \end{pmatrix} = \begin{bmatrix} \cos \theta & -\sin \theta \\ \sin \theta & +\cos \theta \end{bmatrix} \begin{pmatrix} u'_r \\ v'_r \end{pmatrix} \quad (9)$$

Thus, the resulting momentum equation can be expressed in matrix form as:

$$\begin{aligned}
\frac{\rho_f}{\varepsilon^2} \begin{bmatrix} +\cos\theta & \sin\theta \\ -\sin\theta & \cos\theta \end{bmatrix} \begin{pmatrix} u' \frac{\partial u'}{\partial x'} + v' \frac{\partial u'}{\partial y'} \\ u' \frac{\partial v'}{\partial x'} + v' \frac{\partial v'}{\partial y'} \end{pmatrix} &= \begin{bmatrix} +\cos\theta & \sin\theta \\ -\sin\theta & \cos\theta \end{bmatrix} \begin{pmatrix} -\frac{\partial p'}{\partial x'} \\ -\frac{\partial p'}{\partial y'} \end{pmatrix} \\
+ \mu_{\text{eff}} \begin{bmatrix} +\cos\theta & \sin\theta \\ -\sin\theta & \cos\theta \end{bmatrix} \begin{pmatrix} \frac{\partial^2 u'}{\partial x'^2} + \frac{\partial^2 u'}{\partial y'^2} \\ \frac{\partial^2 v'}{\partial x'^2} + \frac{\partial^2 v'}{\partial y'^2} \end{pmatrix} - \mu_f [K]^{-1} \begin{bmatrix} +\cos\theta & \sin\theta \\ -\sin\theta & \cos\theta \end{bmatrix} \begin{pmatrix} u' \\ v' \end{pmatrix} \\
- \rho_f F \sqrt{[K]^{-1}} \begin{bmatrix} +\cos\theta & \sin\theta \\ -\sin\theta & \cos\theta \end{bmatrix} \begin{pmatrix} u' \\ v' \end{pmatrix} \sqrt{u'^2 + v'^2}
\end{aligned} \quad (10)$$

The multiplication of Eq. (10) by the inverse of the rotation matrix, combined with the substitution of the permeability tensor of the anisotropic porous medium using its expression from Eq. (6), results in the following equation:

$$\begin{aligned}
\frac{\rho_f}{\varepsilon^2} \begin{bmatrix} \cos\theta & -\sin\theta \\ \sin\theta & +\cos\theta \end{bmatrix} \begin{bmatrix} +\cos\theta & \sin\theta \\ -\sin\theta & \cos\theta \end{bmatrix} \begin{pmatrix} u' \frac{\partial u'}{\partial x'} + v' \frac{\partial u'}{\partial y'} \\ u' \frac{\partial v'}{\partial x'} + v' \frac{\partial v'}{\partial y'} \end{pmatrix} \\
= \begin{bmatrix} \cos\theta & -\sin\theta \\ \sin\theta & +\cos\theta \end{bmatrix} \begin{bmatrix} +\cos\theta & \sin\theta \\ -\sin\theta & \cos\theta \end{bmatrix} \begin{pmatrix} -\frac{\partial p'}{\partial x'} \\ -\frac{\partial p'}{\partial y'} \end{pmatrix} \\
+ \mu_{\text{eff}} \begin{bmatrix} \cos\theta & -\sin\theta \\ \sin\theta & +\cos\theta \end{bmatrix} \begin{bmatrix} +\cos\theta & \sin\theta \\ -\sin\theta & \cos\theta \end{bmatrix} \begin{pmatrix} \frac{\partial^2 u'}{\partial x'^2} + \frac{\partial^2 u'}{\partial y'^2} \\ \frac{\partial^2 v'}{\partial x'^2} + \frac{\partial^2 v'}{\partial y'^2} \end{pmatrix} \\
- \mu_f \begin{bmatrix} \cos\theta & -\sin\theta \\ \sin\theta & +\cos\theta \end{bmatrix} \begin{bmatrix} 1/K_2 & 0 \\ 0 & 1/K_1 \end{bmatrix} \begin{bmatrix} +\cos\theta & \sin\theta \\ -\sin\theta & \cos\theta \end{bmatrix} \begin{pmatrix} u' \\ v' \end{pmatrix} \\
- \rho_f F \begin{bmatrix} \cos\theta & -\sin\theta \\ \sin\theta & +\cos\theta \end{bmatrix} \begin{bmatrix} 1/\sqrt{K_2} & 0 \\ 0 & 1/\sqrt{K_1} \end{bmatrix} \begin{bmatrix} +\cos\theta & \sin\theta \\ -\sin\theta & \cos\theta \end{bmatrix} \begin{pmatrix} u' \\ v' \end{pmatrix} \sqrt{u'^2 + v'^2}
\end{aligned} \quad (11)$$

Therefore,

$$\begin{aligned}
\frac{\rho_f}{\varepsilon^2} \begin{pmatrix} u' \frac{\partial u'}{\partial x'} + v' \frac{\partial u'}{\partial y'} \\ u' \frac{\partial v'}{\partial x'} + v' \frac{\partial v'}{\partial y'} \end{pmatrix} &= \begin{pmatrix} -\frac{\partial p'}{\partial x'} \\ -\frac{\partial p'}{\partial y'} \end{pmatrix} + \mu_{\text{eff}} \begin{pmatrix} \nabla^2 u' \\ \nabla^2 v' \end{pmatrix} - \frac{\mu_f}{K_1} \begin{bmatrix} K^* \cos^2\theta + \sin^2\theta & (K^* - 1) \sin\theta \cos\theta \\ (K^* - 1) \sin\theta \cos\theta & S^* \sin^2\theta + \cos^2\theta \end{bmatrix} \begin{pmatrix} u' \\ v' \end{pmatrix} \\
- \frac{\rho_f F}{\sqrt{K_1}} \begin{bmatrix} \sqrt{K^*} \cos^2\theta + \sin^2\theta & (\sqrt{K^*} - 1) \sin\theta \cos\theta \\ (\sqrt{K^*} - 1) \sin\theta \cos\theta & \sqrt{K^*} \sin^2\theta + \cos^2\theta \end{bmatrix} \begin{pmatrix} u' \\ v' \end{pmatrix} \sqrt{u'^2 + v'^2}
\end{aligned} \quad (12)$$

The projections of Eq. (12) in the x' direction and in the y' direction yield:

$$\begin{aligned}
\frac{\rho_f}{\varepsilon^2} \left(u' \frac{\partial u'}{\partial x'} + v' \frac{\partial u'}{\partial y'} \right) &= -\frac{\partial p'}{\partial x'} + \mu_{\text{eff}} \left(\frac{\partial^2 u'}{\partial x'^2} + \frac{\partial^2 u'}{\partial y'^2} \right) \\
- \left\{ \frac{\mu_f}{K_1} (K^* \cos^2\theta + \sin^2\theta) + \rho_f \frac{F}{\sqrt{K_1}} (\sqrt{K^*} \cos^2\theta + \sin^2\theta) \sqrt{u'^2 + v'^2} \right\} u' \\
- \left\{ \frac{\mu_f}{K_1} (K^* - 1) \sin\theta \cos\theta + \rho_f \frac{F}{\sqrt{K_1}} (\sqrt{K^*} - 1) \sin\theta \cos\theta \sqrt{u'^2 + v'^2} \right\} v'
\end{aligned} \quad (13)$$

$$\begin{aligned}
\frac{\rho_f}{\varepsilon^2} \left(u' \frac{\partial v'}{\partial x'} + v' \frac{\partial v'}{\partial y'} \right) &= -\frac{\partial p'}{\partial y'} + \mu_{\text{eff}} \left(\frac{\partial^2 v'}{\partial x'^2} + \frac{\partial^2 v'}{\partial y'^2} \right) \\
- \left\{ \frac{\mu_f}{K_1} (K^* - 1) \sin\theta \cos\theta + \rho_f \frac{F}{\sqrt{K_1}} (\sqrt{K^*} - 1) \sin\theta \cos\theta \sqrt{u'^2 + v'^2} \right\} u' \\
- \left\{ \frac{\mu_f}{K_1} (K^* \sin^2\theta + \cos^2\theta) + \rho_f \frac{F}{\sqrt{K_1}} (\sqrt{K^*} \sin^2\theta + \cos^2\theta) \sqrt{u'^2 + v'^2} \right\} v'
\end{aligned} \quad (14)$$

2.2.3 Heat transfer

The energy equation can be expressed for the fluid and the porous region, respectively, as follows:

$$(\rho C_p)_f \left(u' \left(\frac{\partial T'}{\partial x'} \right) + v' \left(\frac{\partial T'}{\partial y'} \right) \right) = k_f \left(\frac{\partial^2 T'}{\partial x'^2} + \frac{\partial^2 T'}{\partial y'^2} \right) \quad (15)$$

$$(\rho C_p)_f \left(u' \left(\frac{\partial T'}{\partial x'} \right) + v' \left(\frac{\partial T'}{\partial y'} \right) \right) = k_f \left(\frac{\partial^2 T'}{\partial x'^2} + \frac{\partial^2 T'}{\partial y'^2} \right) \quad (16)$$

where, $(\rho C_p)_f$ denotes the fluid volumetric heat capacity (product of the fluid density and the fluid specific heat capacity), and k_f refers to the fluid thermal conductivity.

2.2.4 Boundary conditions

As shown in Figure 1, the appropriate boundary conditions associated with the above equations are:

$$\text{At } x' = 0 \text{ (inlet)} \quad \begin{cases} u' = u'_e = u'_{av}, & v' = v'_e = 0 \\ T' = T'_e \end{cases} \quad (17)$$

$$\text{At } x' = l \text{ (outlet)} \quad \begin{cases} \partial u' / \partial x' = 0, & \partial v' / \partial x' = 0 \\ (\partial T' / \partial x') = 0 \end{cases} \quad (18)$$

$$\text{At } y' = 0 \text{ (imposed flux)} \quad \begin{cases} u' = 0, & v' = 0 \\ (\partial T' / \partial y') = -q_w / k_{eff} \end{cases} \quad (19)$$

$$\text{At } y' = H \text{ (symmetry axis)} \quad \begin{cases} \partial u' / \partial y' = 0, & v' = 0 \\ (\partial T' / \partial y') = 0 \end{cases} \quad (20)$$

$$\text{At } y' = e_p \text{ (Interface fluid/porous layer)} \quad \begin{cases} u'_f = u'_p, & v'_f = v'_p \\ \mu_f \frac{\partial u'_f}{\partial y'} = \mu_{eff} \frac{\partial u'_p}{\partial y'}, \\ \mu_f \frac{\partial v'_f}{\partial y'} = \mu_{eff} \frac{\partial v'_p}{\partial y'} \\ T'_f = T'_p, \\ k_f (\partial T' / \partial y')|_f = k_{eff} (\partial T' / \partial y')|_p \end{cases} \quad (21)$$

At the interface, the fluid is in local thermal equilibrium with the porous layer. At the inlet of channel, the velocity component in the x-direction is assumed to be a prescribed average velocity u'_{av} .

2.3 Dimensionless Form for the Governing Equations

The adopted dimensionless coordinates and variables, along with the dimensionless parameters, are introduced into the above equations, specifically

$$\begin{cases} x = x'/H, & y = y'/H \\ u = u'/u'_{av}, & v = v'/\bar{u}' \\ p = p' / (\rho_f u'_{av}{}^2) \\ T = (T' - T'_e) / \Delta T' \end{cases} \quad (22)$$

$$Re = u'_{av} H / \nu_f, \nu_{eff} = \mu_{eff} / \rho_f, \nu_f = \mu_f / \rho_f$$

where, u , v , p and T denote the dimensionless components of velocity, pressure, and temperature, respectively. Re denotes the Reynolds number and ν_{eff} the effective kinematic viscosity of the porous layer. This leads to the following dimensionless form of the governing equations:

2.3.1 Fluid flow

For the fluid region, the dimensionless continuity equation and the dimensionless conservation equations of momentum in the fluid are given as follows:

$$u \frac{\partial u}{\partial x} + v \frac{\partial u}{\partial y} = 0 \quad (23)$$

$$u \frac{\partial u}{\partial x} + v \frac{\partial u}{\partial y} = -\frac{\partial p}{\partial x} + \frac{1}{Re \left(\frac{\partial^2 u}{\partial x^2} + \frac{\partial^2 u}{\partial y^2} \right)} \quad (24)$$

$$u \frac{\partial v}{\partial x} + v \frac{\partial v}{\partial y} = -\frac{\partial p}{\partial y} + \frac{1}{Re \left(\frac{\partial^2 v}{\partial x^2} + \frac{\partial^2 v}{\partial y^2} \right)} \quad (25)$$

Similarly, for the porous region, the dimensionless conservation equations of momentum are given as follows:

$$\begin{aligned} u \frac{\partial u}{\partial x} + v \frac{\partial u}{\partial y} &= -\varepsilon^2 \frac{\partial p}{\partial x} + \varepsilon^2 \frac{R_v^*}{Re} \left(\frac{\partial^2 u}{\partial x^2} + \frac{\partial^2 u}{\partial y^2} \right) \\ &- \left[\frac{\varepsilon^2}{ReDa} (K^* \cos^2 \theta + \sin^2 \theta) + \frac{F\varepsilon^2}{\sqrt{Da}} \left(\sqrt{K^*} \cos^2 \theta + \sin^2 \theta \right) \sqrt{u^2 + v^2} \right] u \\ &- \left[\frac{\varepsilon^2}{ReDa} (K^* - 1) \sin \theta \cos \theta + \frac{F\varepsilon^2}{\sqrt{Da}} \left(\sqrt{K^*} - 1 \right) \sin \theta \cos \theta \sqrt{u^2 + v^2} \right] v \end{aligned} \quad (26)$$

$$\begin{aligned} u \frac{\partial v}{\partial x} + v \frac{\partial v}{\partial y} &= -\varepsilon^2 \frac{\partial p}{\partial y} + \varepsilon^2 \frac{R_v^*}{Re \left(\frac{\partial^2 v}{\partial x^2} + \frac{\partial^2 v}{\partial y^2} \right)} \\ &- \left[\frac{\varepsilon^2}{ReDa} (K^* - 1) \sin \theta \cos \theta + \frac{F\varepsilon^2}{\sqrt{Da}} \left(\sqrt{K^*} - 1 \right) \sin \theta \cos \theta \sqrt{u^2 + v^2} \right] u \\ &- \left[\frac{\varepsilon^2}{ReDa} (K^* \sin^2 \theta + \cos^2 \theta) + \frac{F\varepsilon^2}{\sqrt{Da}} \left(\sqrt{K^*} \sin^2 \theta + \cos^2 \theta \right) \sqrt{u^2 + v^2} \right] v \end{aligned} \quad (27)$$

2.3.2 Heat transfer

In dimensionless form, the energy conservation equations in the fluid and the porous region are respectively given by:

$$u \frac{\partial T}{\partial x} + v \frac{\partial T}{\partial y} = \frac{1}{Pr Re \left(\frac{\partial^2 T}{\partial x^2} + \frac{\partial^2 T}{\partial y^2} \right)} \quad (28)$$

$$u \frac{\partial T}{\partial x} + v \frac{\partial T}{\partial y} = \frac{R_k^*}{Pr Re \left(\frac{\partial^2 T}{\partial x^2} + \frac{\partial^2 T}{\partial y^2} \right)} \quad (29)$$

where, Pr refers to the Prandtl number.

2.3.3 Dimensionless form of boundary conditions

In dimensionless form, the boundary conditions, given above by Eqs. (17)–(22), are written as follows:

$$\text{At } x = 0 \text{ (inlet)} \quad \begin{cases} u = 1, & v = 0 \\ T = 0 \end{cases} \quad (30)$$

$$\text{At } x = \frac{l}{H} = L^* \text{ (outlet)} \quad \begin{cases} \partial u / \partial x = 0, & \partial v / \partial x = 0 \\ \partial T / \partial x = 0 \end{cases} \quad (31)$$

$$\text{At } y = 0 \text{ (imposed flux)} \begin{cases} u = 0, & v = 0 \\ \partial T / \partial y = -1 / R_k^* \end{cases} \quad (32)$$

$$\text{At } y = 1 \text{ (Symmetry axis)} \begin{cases} (\partial u / \partial y) = 0, & v = 0 \\ (\partial T / \partial y) = 0 \end{cases} \quad (33)$$

$$\text{At } y = \frac{e_p}{H} = E^* \text{ (Interface fluid/porous layer)} \begin{cases} u_f = u_p, & v_f = v_p \\ \frac{\partial u_f}{\partial y} = R_v^* \frac{\partial u_p}{\partial y}, \\ \frac{\partial v_f}{\partial y} = R_v^* \frac{\partial v_p}{\partial y} \\ T_f = T_p, & \frac{\partial T_f}{\partial y} = R_k^* \frac{\partial T_p}{\partial y} \end{cases} \quad (34)$$

where, u , v , p , and T denote the dimensionless components of velocity, pressure, and temperature, respectively. Re denotes the Reynolds number and v_{eff} the effective kinematic viscosity of the porous layer.

2.4 Definition of Other Required Parameters

In this study, the average velocity and average temperature are respectively defined as follows:

$$u'_{\text{av}} = \frac{1}{\rho[H \times 1]} \int_0^H (\rho u') dy' \text{ and } T'_{\text{av}} = \frac{1}{H u'_{\text{av}}} \int_0^H (u' T') dy' \quad (35)$$

In dimensionless form, the above quantities are expressed as follows:

$$u_{\text{av}} = \int_0^1 u dy \text{ and } T_{\text{av}} = \frac{1}{u_{\text{av}}} \int_0^1 (uT) dy \quad (36)$$

Furthermore, the coefficient of friction of a fluid flow is defined as [15]:

$$f' = 2H (-\partial p' / \partial x') / (\rho_f (u'_e)^2 / 2) \quad (37)$$

Using dimensionless variables, one can find: $f = 4(-\partial p / \partial x)$, which implies

$$f \times (Re)_{2H} = f(Re)_{2H} = 4 \left(-\frac{\partial p}{\partial x} \right) \left(\frac{u'_e (2H)}{v_f} \right) = 8 Re \left(-\frac{\partial p}{\partial x} \right) \quad (38)$$

Likewise, for flow in a channel partially filled with a porous medium, the Nusselt number is defined as: $Nu = h \times 2H / k_{\text{eff}}$ [16]; the local convective heat transfer coefficient (h) can be calculated using: $h = 2q_w / (T'_w - T'_{\text{av}})$. Thus, the Nusselt number is expressed as:

$$Nu = 4H \times q_w / k_{\text{eff}} (T'_w - T'_{\text{av}}) \quad (39)$$

Using dimensionless parameters, one can write:

$$Nu = 4 / R_k^* (T_w - T_{\text{av}}) \quad (40)$$

The average Nusselt number along the channel is calculated as follows:

$$Nu_{\text{av}} = \frac{1}{L^*} \int_0^{L^*} Nu(x) dx \quad (41)$$

Recall that $L^* = l / H$ represents the aspect ratio of the channel.

2.5 Dimensionless Control Parameters Characterizing the Studied Problem

To validate the present model, we consider the following fixed dimensionless control parameters: $Pr = 0.7$, $Re = 100$, $R_v^* = 1$, and $L^* = l/H = 50$ (see Table 1). All calculations in this study use these parameters, with air as the tested fluid, laminar flow, and a fixed porosity of $\varepsilon = 0.9$. Alternative values can be selected, and most calculations explore varying values of F , anisotropic hydrodynamic parameters (K^* and θ), and other factors influencing hydrodynamic anisotropy, including Da and E^* (with two values of R_k^* examined). These dimensionless quantities characterize forced convection fluid flow in a channel partially filled with an anisotropic porous layer (Figure 1), and their values are summarized in Table 1.

Table 1. Dimensionless control parameters for fluid and porous medium used in the numerical calculations

Parameter	Value	Comment/Assumption
Aspect ratio, $L^* = l/H$	50	Fully developed flow
Prandtl number, Pr	0.7	Air as tested fluid
Reynolds number, Re	100	To ensure laminar flow regime
Ratio of the kinematic viscosities, R_v^*	1	μ_{eff} is identical to μ_f
Ratio of the thermal conductivities, R_k^*	1 and 0.1	Tested values
Forchheimer inertia coefficient, F	0, 0.1, 1	Tested values
Darcy number, Da	$(10^{-4} \leq Da \leq 10^{-1})$	Tested values
Dimensionless thickness of the layer, E^*	0, 0.2, 0.4, 0.6, 0.8, and 1	Tested values
Anisotropic permeability ratio, K^*	0.25, 1, and 5	$K^* < 1$, $K^* = 1$, $K^* > 1$
Porosity, ε	0.9	Fixed porosity
Anisotropy orientation angle, θ	$0^\circ, 30^\circ, 60^\circ, 90^\circ, 120^\circ, 150^\circ, 180^\circ$	Tested values

3 Numerical Resolution

3.1 Resolution Procedure

To solve the system of coupled equations and the associated boundary conditions, described by Eqs. (23)–(34), a numerical code in Fortran was developed. This code uses a method based on the finite volume technique [31], chosen to transform the system of governing equations (partial differential equations) into a set of algebraic equations that are easier to solve. Power law schemes are applied for the discretization of the governing equations, while the SIMPLE algorithm [31] is used to link pressure to velocity.

In applying the SIMPLE algorithm, particular attention was given to the sequential resolution of temperature. The resulting discretized equations essentially form a system of tridiagonal algebraic equations, which is solved iteratively by double sweeping using the Thomas algorithm (TDMA) [31]. To accelerate convergence, the velocity components are under-relaxed by a factor of 0.9, pressure by a factor of 0.5, and temperature by a factor of 1.1. A uniform grid is used to ensure that the results are independent of the grid size (as illustrated below).

On the other hand, to verify convergence at each mesh node, we conduct a convergence test by comparing the values of the dependent variable ϕ (where ϕ represents u , v and T) across iterations. Convergence is achieved when the relative error of ϕ is below a specified threshold, calculated as $\max |(\phi - \phi^*) / \phi^*| \leq \xi$, where ϕ^* is the value from the previous iteration. In this study, we set the threshold ξ to 10^{-7} for u , v and T .

3.2 Mesh Independence Study

To perform a mesh independence study and ensure the accuracy of the numerical results, we consider the problem of forced convection fluid flow in a flat horizontal channel partially filled with an anisotropic porous matrix (shown in Figure 1). Two cases are studied:

Case A: Parameters ($K^* = 1$ and $\theta = 0^\circ$), along with ($Da = 10^5$ and $E^* = 0$) and ($F = 0$ and $R_k^* = 1$), represent a channel without a porous medium. In this scenario, the flow is characterized as a “clear fluid” and is associated with the Poiseuille phenomenon.

Case B: This case involves parameters ($K^* = 0.1$ and $\theta = 90^\circ$), along with ($Da = 10^{-1}$ and $E^* = 0$) and ($F = 0$ and $R_k^* = 1$), representing the problem of fully developed fluid flow in an anisotropic porous medium.

The values of the control parameters characterizing cases A and B are summarized in Table 2.

The equations governing these two cases were solved on different mesh sizes: 161×21 , 161×41 , 181×41 , 181×51 , 201×51 and 221×51 . The objective is to ensure that the results (particularly Nu and u_{max} , where u_{max} is the maximum value of the streamwise velocity) are independent of the grid size. The numerical results for Cases A and B are presented in Table 3 and Table 4, respectively.

Simulations show that 80,000 iterations are sufficient to obtain a convergent solution with a grid of 201×51 nodes (see Table 3 and Table 4). Thus, for all the results presented below, the mesh used consists of 201×51 nodes.

Table 2. Values of control parameters used in study cases A, B and C

Parameter	Case A	Case B	Case C
Aspect ratio, $L^* = l/H$	50	50	50
Prandtl number, Pr	0.7	0.7	0.7
Reynolds number, Re	100	100	100
Ratio of the kinematic viscosities, R_v^*	0	$\ll 1$	1
Ratio of the thermal conductivities, R_k^*	0	$\ll 1$	1
Forchheimer inertia coefficient, F	0	0	0 and 0.1
Darcy number, Da	$\gg 1$ (ex. 10^5)	10^{-1}	10^{-3}
Dimensionless thickness of the layer, E^*	0	1	1
Anisotropic permeability ratio, K^*	NA [#]	0.1	0.25 and 5
Porosity, ε	NA	0.9	0.9
Anisotropy orientation angle, θ	NA	90°	0°, 30°, 60°, 90°, 120°, 150°, 180°

Table 3. Mesh independence study: Flow and heat transfer results (Case A: poiseuille flow, $Da = 10^5$)

Mesh Size ($x \times y$)	161 × 21	181 × 41	201 × 51*	221 × 61
Maximum streamwise velocity, u_{\max}	1.4631	1.4799	1.4823	1.4827
Error (%)	-	1.1482	0.1622	0.0270
Nusselt number, Nu	8.4246	8.3385	8.3204	8.3209
Error (%)	-	1.0220	0.2171	0.00361

Table 4. Effect of mesh refinement on flow and heat transfer in an anisotropic porous channel. Numerical predictions for a fully filled channel of an anisotropic porous medium (Case B: $Da = 10^{-1}$, $K^* = 0.25$, $\theta = 90^\circ$)

Mesh Size ($x \times y$)	161 × 21	181 × 41	201 × 51*	221 × 61
Maximum streamwise velocity, u_{\max}	1.3133	1.3227	1.3241	1.3245
Error (%)	-	0.7158	0.1058	0.03021
Nusselt number, Nu	9.0096	8.9506	8.9364	8.9370
Error (%)	-	0.6549	0.1586	0.00671

3.3 Comparison of the Present Model with Available Analytical Solutions

The validation of this model is carried out through the following comparisons:

- **Comparison with the analytical study by White [32]:** The fully developed axial velocity profile for Poiseuille flow (Case A) is validated against the analytical solution of the study [32], as illustrated in Figure 2 and Table 5. Only the lower half of the channel is shown, the problem being symmetric about the centerline.

- **Comparison with the analytical study by Degan et al. [21]:** The fully developed axial velocity profile for Case B is validated against the analytical solution of the study [21], as illustrated in Figure 3 and Table 6.

The fully developed velocity profiles predicted by the model for both Case A and Case B demonstrate acceptable agreement with the analytical solutions (see Figure 2 and Figure 3). Additionally, Table 5 and Table 6 indicate good alignment between the numerical results obtained and those reported in the literature for both cases.

Table 5. Poiseuille flow (Case A): Comparison of the present model results with White's analytical study [32]

Controlling Number	Present Model		White [32]	
Da	u_{\max}	Nu	u_{\max}	Nu
10^5	1.4823	8.3204	1.5000	8.2350

Table 6. Fully developed velocity profile in the anisotropic porous medium (Case B): Comparison of model results with the analytical study by Degan et al. [21]

Controlling Number	Present Model (Case B)		Degan et al. [21]	
Da	u_{\max}	Nu	u_{\max}	Nu
10^{-1}	1.3241	8.9364	1.3367	8.8612

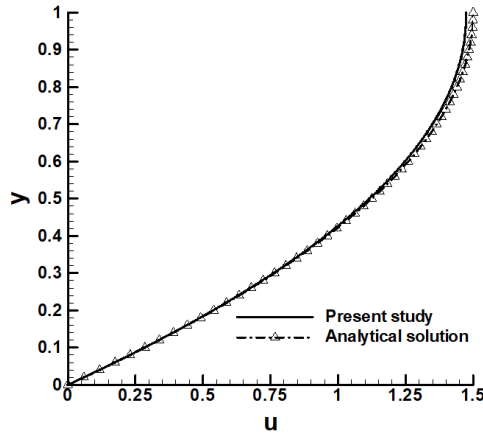


Figure 2. Validation of Poiseuille flow (Case A): Fully developed velocity profile compared to White’s analytical solution [32]

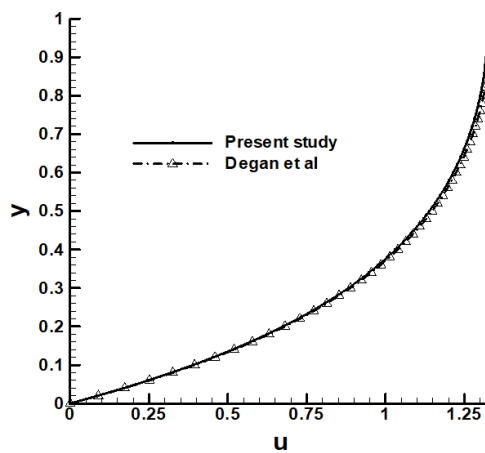


Figure 3. Fully developed velocity profile in an anisotropic porous layer (Case B)

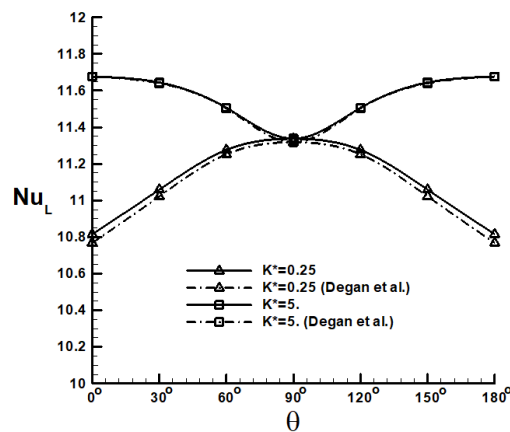


Figure 4. Case C: Comparison of the variation of the Nusselt number as a function of the anisotropy orientation angle θ predicted by the present model with results from the analytical study [21]

Further comparison of the present model was conducted by examining another aspect of the analytical study [21], which investigates the effect of varying the anisotropy orientation angle on the Nusselt number (without the influence of the inertia term, setting $F = 0$) in a completely filled channel (i.e., $E^* = 1$).

In this analysis (Case C), the parameters considered are ($K^* = 0.25$ and $K^* = 5$) and $Da = 10^{-3}$. Additionally, two cases for F are evaluated ($F = 0$ and $F = 0.1$) with $R_k^* = 1$ (see Table 2). The results of this comparison are illustrated in Figure 4.

The findings from Figure 4, predicted by the present model, align well with the analytical study of [21]. Particularly, the variation of the Nusselt number in relation to the anisotropy orientation angle, for $Fo = 0$, closely matches the analytical solution from the study [21]. This leads to the conclusion that the Forchheimer inertia term has minimal impact on fluid flow and heat transfer in a channel completely filled with an anisotropic porous medium.

This observation may clarify the frequent omission of the Forchheimer inertia term in earlier studies addressing forced convective fluid flow in such channels, particularly those characterized by low permeability. Therefore, for low permeabilities, the exclusion of the inertia term from the governing equations can be justified without significantly affecting the results (see Figure 4).

4 Results and Discussion

4.1 First Part

In this first part of the study, we focus on two main objectives:

- **Effect of Forchheimer inertia term on heat transfer:** We highlight the impact of the inertia term on heat transfer characteristics in the channel by examining various permeability values of an assumed isotropic porous layer.

- **Influence of anisotropic parameters:** We explore the effects of key anisotropic hydrodynamic parameters, particularly the anisotropic permeability ratio (K^*) and the anisotropy orientation angle (θ), on the heat transfer and flow characteristics of the fluid. This involves setting specific values for permeability (Da) and layer thickness (E^*).

Furthermore, we pay particular attention to other complementary parameters that may influence the hydrodynamic anisotropy of the porous medium, such as the thickness of the inserted layer and its effective thermal conductivity (k_{eff}). For this analysis, a fixed permeability value (Da) was chosen, and two values of the ratio of thermal conductivities ($R_k^* = k_{eff}/k_f$) were tested.

4.1.1 Effect of Forchheimer inertia coefficient on heat transfer

To study the effect of the Forchheimer inertia coefficient (F) of the porous layer on the heat transfer characteristics in the channel, we revisit the physical problem depicted in Figure 1, which illustrates forced convection fluid flow in a channel filled with an isotropic porous layer. We will consider the following two channel cases:

- **Channel entirely filled with an isotropic porous layer ($E^* = 1$)**

In the case where the thickness of the layer is unity ($E^* = 1$), the channel depicted in Figure 1 is completely filled with the porous medium. The variations of the Nusselt number for fully developed laminar flow, predicted for $K^* = 1$ and $\theta = 0^\circ$ (isotropic case), are shown in Figure 5. Predictions have been made for different values of the Forchheimer inertia term (corresponding to $F = 0, 0.1, \text{ and } 1$).

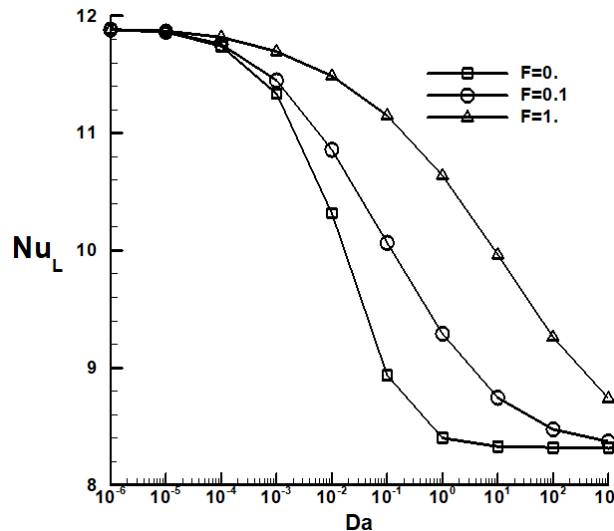


Figure 5. Variations of the Nusselt number in terms of the Darcy number (Da) in the fully developed region of the fully filled channel: Predictions were made for different values of F (0, 0.1 and 1) and with $K^* = 1$ and $\theta = 0^\circ$

As illustrated in Figure 5, for $F = 0$ and $F = 0.1$, it is observed that as the permeability of the medium increases (in the range $10^{-4} \leq Da \leq 10^3$), the Nusselt number decreases and becomes independent of Fo when the permeability exceeds 10^3 (i.e., $Da > 10^3$). Physically, this indicates that when the permeability of the porous medium surpasses 10^3 , the porosity effectively disappears, allowing flow to develop in the channel without the porous medium. Consequently, the Nusselt number becomes independent of Fo and asymptotically approaches Nu

= 8.3209 (see Figure 5), which is very close to the value for fully developed flow in a channel without a porous medium ($Nu = 8.3204$).

For $F = 1$, Figure 5 shows that when the permeability is significant (10^3), Nu is approximately 8.7400, which also aligns well with the value for flow in a channel without a porous medium. However, for lower permeability values, particularly $Da \leq 10^{-4}$, the results indicate that Nu becomes progressively independent of F due to the channeling effect [33]. Specifically, the influence of the inertia term on the Nusselt number diminishes as permeability decreases and becomes negligible for $Da \leq 10^{-5}$, approaching the limit case of $Nu = 11.8832$. Therefore, in a channel entirely filled with a porous medium, the effect of the inertia term on the Nusselt number can be disregarded for permeability values less than or equal to 10^{-4} (i.e., $Da \leq 10^{-4}$).

• **Channel partially filled with an isotropic porous layer ($E^* = 0.6$)**

In the case where the thickness of the layer is $E^* = 0.6$, the channel depicted in Figure 1 is partially filled with the porous layer. The variations of the Nusselt number for fully developed laminar flow, predicted for $K^* = 1$ and $\theta = 0^\circ$, are illustrated in Figure 6. Predictions were made with different values of the Forchheimer inertia coefficient ($F = 0, 0.1, \text{ and } 1$) and with the ratio of thermal conductivities $R_k^* = 1$.

As shown in Figure 6, with an increase in permeability (in the range $10^{-4} \leq Da \leq 10^3$), the Nusselt number also increases, becoming independent of F when the permeability reaches a significant value. Specifically, for $Da = 10^3$, the Nusselt number Nu approaches the value for flow in a channel without the porous layer ($Nu = 8.3204$) and becomes independent of F .

As Darcy number decreases from 10^3 to 10^{-4} , the flow rate in the porous layer decreases, resulting in differences in Nusselt number values for $F = 0, 0.1, \text{ and } 1$. This variation is attributed to the inertia effect [34]. For values of $Da \leq 10^{-4}$, the Nusselt number becomes independent of F , indicating that in a channel partially filled with a porous medium, the effect of the inertia term can also be neglected for permeability values less than or equal to 10^{-4} .

In conclusion, the results suggest that in channels completely or partially filled with a porous medium, the Forchheimer inertia coefficient does not significantly influence the Nusselt number for porous media with $Da \leq 10^{-4}$. This finding explains why this coefficient is often overlooked in previous numerical studies, where low permeability values were considered.

Remark: As shown in Figure 6, the effect of the Forchheimer inertia coefficient (F) on heat transfer disappears for porous media with $Da \leq 10^{-4}$. It begins to emerge, albeit insignificantly, as Da increases, particularly in the range $10^{-4} \leq Da \leq 10^3$. The influence of this coefficient gradually becomes noticeable when $Da \geq 10^{-3}$ and is clearly observable for values exceeding $Da > 10^{-2}$.

The value $F = 0.1$ is particularly suitable for achieving good results when Da is in the interval $10^{-4} \leq Da \leq 10^{-2}$ and provides acceptable results for $10^{-2} \leq Da \leq 10^{-1}$ (see Figure 6). Therefore, in all subsequent calculations (primarily conducted with $Da = 10^{-3}, 10^{-2}, \text{ or } 10^{-1}$) the Forchheimer inertia coefficient will be set to $F = 0.1$.

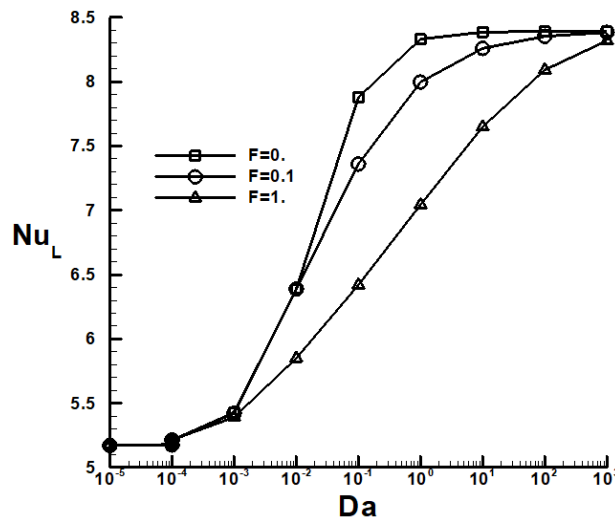


Figure 6. Nusselt number as a function of the Darcy number (Da) in the fully developed region for different values of F (0, 0.1 and 1): Prediction with $K^* = 1$ and $\theta = 0^\circ$ in the partially filled channel with $E^* = 0.6$

4.1.2 Influence of anisotropic parameters

Now, to investigate the effects of the anisotropic hydrodynamic parameters (mainly K^* and θ) of the porous medium on fluid flow and heat transfer characteristics, we will revisit the problem illustrated in Figure 1. In this case, we consider the thickness of the porous layer as $E^* = 0.6$ and the Darcy number as $Da = 10^{-3}$.

• **Effect of the anisotropic permeability ratio K^***

The variations of the velocity and temperature profiles in the established region, based on the anisotropic permeability ratio, are shown in Figure 7a and Figure 7b, respectively. The variations of the Nusselt number and the coefficient of friction along the channel as functions of K^* are illustrated in Figure 7c and Figure 7d. Predictions were made for K^* values of 0.25, 1, and 5, with $Da = 10^{-3}$, $\theta = 0^\circ$, $F = 0.1$, and $R_k^* = 1$. Analysis of these figures shows:

(1) Velocity profiles: Figure 7a indicates that the position of the velocity profiles along the channel axis depends on the value of K^* , with the maximum velocity occurring at $K^* = 5$. When $K^* < 1$ (which implies $K_1 = 1$, see Figure 1), the strength of the convective flow in the porous layer is enhanced compared to the isotropic case ($K^* = 5$). Conversely, when $K^* > 1$, the effectiveness of convective movement diminishes, leading to a significant portion of the flow escaping in the fluid region. This is due to the lower permeability in the flow direction (K_2) compared to the vertical one (K_1).

(2) Temperature profiles: Similarly, Figure 7b shows that the predicted temperature profiles exhibit behavior akin to the velocity distributions in the porous layer. In the case of $K^* = 0.25$, the small difference between the wall temperature and the average temperature suggests a higher expected Nusselt number in the developed region. This trend is further supported by the variations in the Nusselt number along the channel in terms of K^* (see Figure 7c), where it is observed that Nu decreases as K^* increases.

(3) Coefficient of friction: In contrast to the variations of Nu , the coefficient of friction exhibits an opposite trend (see Figure 7d).

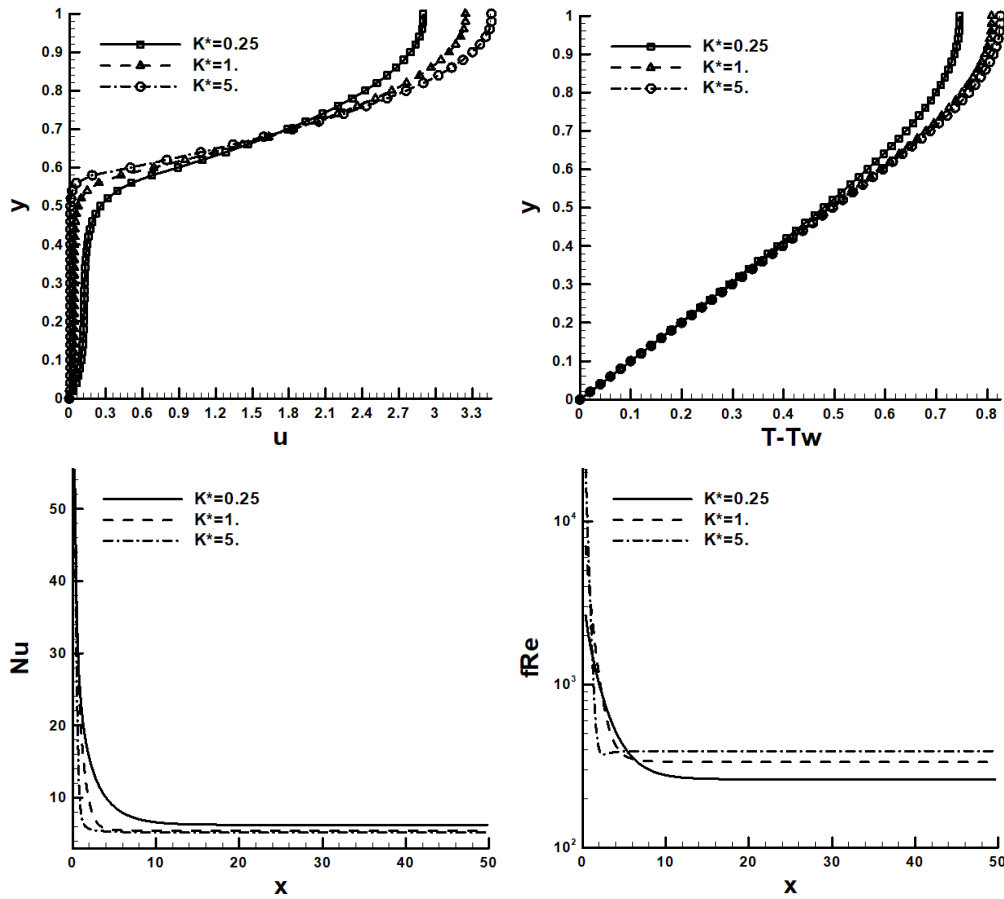


Figure 7. Effect of permeability ratio K^* (0.25, 1 and 5) on the flow and heat transfer characteristics in the partially filled channel: $E^* = 0.6$, $\theta = 0^\circ$, $Da = 10^{-3}$, $F = 0.1$, and $R_k^* = 1$: (a) velocity profiles; (b) temperature profiles; (c) Nusselt number; and (d) friction coefficient

• **Effect of the anisotropy orientation angle θ for different values of the ratio K^***

Similar to the previous case, predictions were made for different values of the anisotropy orientation angle: 0° , 30° and 90° . The porous medium has a Darcy number of $Da = 10^{-3}$, the Forchheimer inertia coefficient was set to $F = 0.1$, and the thermal conductivities ratio was considered. Furthermore, to account for the effect of the anisotropic permeability ratio, two cases for K^* were examined: one where $K^* < 1$ (e.g., $K^* = 0.25$) and another where $K^* >$

1 (e.g., $K^* = 5$).

(1) Case where $K^* < 1$

For $K^* = 0.25$, the variations of velocity and temperature profiles based on the anisotropy orientation angle are presented in Figure 8a and Figure 8b. The variations of the Nusselt number and the friction coefficient along the channel as a function of θ are shown in Figure 8c and Figure 8d. An examination of Figure 8a to Figure 8d reveals the following:

The velocity profiles in Figure 8a indicate that convective flow intensity is maximized at $\theta = 0^\circ$ and minimized at $\theta = 90^\circ$, aligning the porous layer's principal axis with the flow direction. This trend reverses in the clear fluid region. Notably, the flow model in a partially filled channel ($E^* = 0.6$) resembles that of a fully filled porous layer ($E^* = 1$) (see the study [21]).

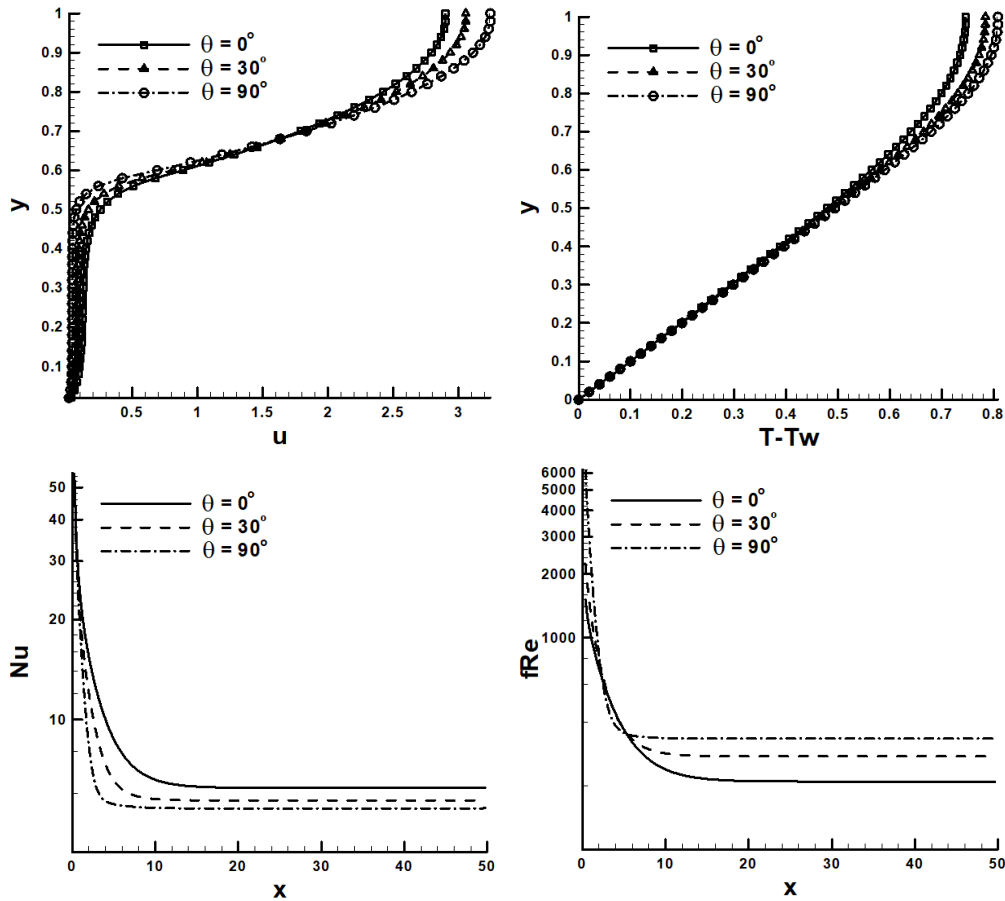


Figure 8. Effect of anisotropy orientation angle θ (0° , 30° , 90°) on the flow and heat transfer characteristics in the partially filled channel: $E^* = 0.6$, Case ($K^* \leq 1$): $K^* = 0.25$, $Da = 10^{-3}$, $F = 0.1$, $R_k^* = 1$: (a) velocity profiles; (b) temperature profiles; (c) Nusselt number; and (d) friction coefficient

The temperature profile at $\theta = 0^\circ$ (Figure 8b) shows a small difference between the wall and average temperatures, suggesting a higher Nusselt number in the developed region, as illustrated in Figure 8c, where Nusselt values increase with decreasing anisotropy orientation angle.

Finally, the friction coefficient distributions in Figure 8d exhibit an inverse trend compared to the Nusselt number.

(2) Case where $K^* > 1$

For $K^* = 5$, the variations of the velocity and temperature profiles as a function of the anisotropy orientation angle are presented in Figure 9a and Figure 9b, respectively. The variations of the Nusselt number and the friction coefficient along the channel as a function of θ are illustrated in Figure 9c and Figure 9d.

The velocity profiles in Figure 9a show that the intensity of the convective flow is maximized when $\theta = 90^\circ$ and minimized at $\theta = 0^\circ$, indicating that the flow is optimal when the main axis of the anisotropic porous layer is parallel to the flow direction. In contrast, Figure 9b reveals that the temperature profiles exhibit an opposite behavior. At $\theta = 90^\circ$, the small difference between the wall temperature and the average temperature suggests an increased heat transfer, as shown in Figure 9c, where the Nusselt number values increase with the anisotropy orientation angle. Finally, distributions of the friction coefficient in Figure 9d show an inverse trend compared to the Nusselt number.

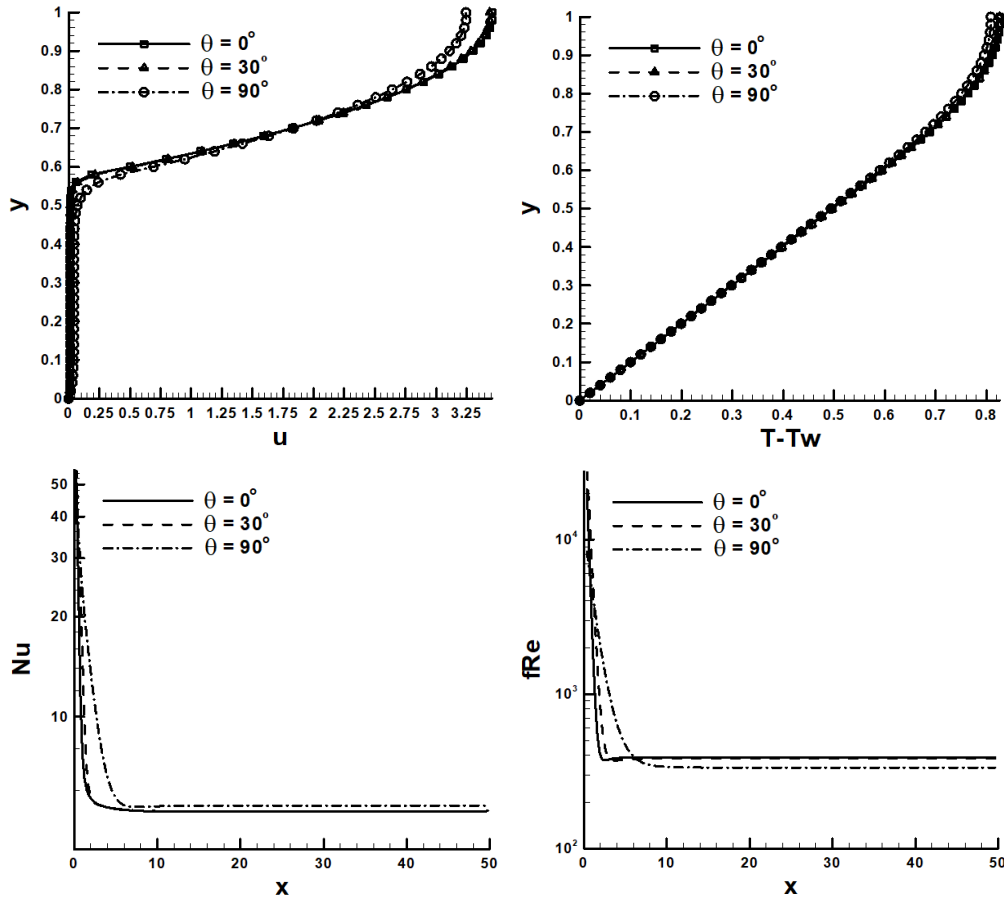


Figure 9. Effect of anisotropy orientation angle θ (0° , 30° , 90°) on the flow and heat transfer characteristics in the partially filled channel: $E^* = 0.6$, Case ($K^* > 1$): $K^* = 5$, $Da = 10^{-3}$, $F = 0.1$, $R_k^* = 1$: (a) velocity profiles; (b) temperature profiles; (c) Nusselt number; and (d) friction coefficient

4.1.3 Effect of porous layer thickness E^* for low and high value of R_k^* ratio on heat transfer and fluid flow characteristics in a partially filled channel

In the following subsection, we pay particular attention to the effects of other parameters that can influence the hydrodynamic anisotropy of the porous layer. We focus primarily on the relationship between thermal conductivities ratio R_k^* and porous medium thickness E^* on fluid flow and heat transfer in a partially filled channel. To study the impact of anisotropic porous layer thickness on fluid flow and heat transfer in the presence of the R_k^* effect, we reconsider the previous calculation case, i.e., when $K^* = 0.25, 1$ and 5 , $\theta = 0^\circ$, $F = 0.1$ and $Da = 10^{-3}$. Several thickness values were considered in these calculations (see Table 1). To evaluate the effect of R_k^* , we examined two values: $R_k^* = 1$ and 0.1 .

• On heat transfer

The variations of the Nusselt number in the established region as a function of porous layer thickness (E^*) for two values of the ratio of thermal conductivities ($R_k^* = 1$ and 0.1) are shown in Figure 10a and Figure 10b.

First case $R_k^* = 1$: Figure 10a indicates that for each K^* , the Nusselt number decreases with increasing thickness, reaching a minimum value termed "optimal". This optimal thickness varies with K^* and is always below the Nusselt number for a channel without a porous layer (8.3204). Beyond this minimum, Nusselt values increase, surpassing those of the channel without a porous layer, peaking at $Nu = 11.7424$.

Second case $R_k^* = 0.1$: In contrast, for $R_k^* = 0.1$, Nusselt values exceed those of $R_k^* = 1$. For thicknesses between 0 and 0.8, the highest Nu occurs when $K^* < 1$. However, for thicknesses greater than 1, this trend reverses (see Figure 10b). Overall, lower effective thermal conductivity (k_{eff}) in porous media is recommended to enhance heat transfer in partially filled channels.

• On fluid flow

The variations in the coefficient of friction in the established region as a function of porous layer thickness (E^*) for two values of the ratio of thermal conductivities ($R_k^* = 1$ and 0.1) are shown in Figure 10c and Figure 10d. Both figures reveal that the coefficient of friction is unaffected by changes in R_k^* , highlighting an advantage of reducing

R_k^* . Additionally, the friction coefficient increases with the thickness of the porous layer. For a given thickness, the highest coefficient corresponds to an anisotropic permeability ratio ($K^* > 1$), indicating that lower permeability in the flow direction results in a higher friction coefficient.

Remark: Analysis of previous subsections shows that anisotropic hydrodynamic parameters, such as Da , θ and E^* , significantly influence fluid flow and heat transfer in partially filled channels. Thus, further study is needed to improve heat transfer using various combinations of anisotropy orientation angle, permeability, and layer thickness. This will be the focus of the next part of this study.

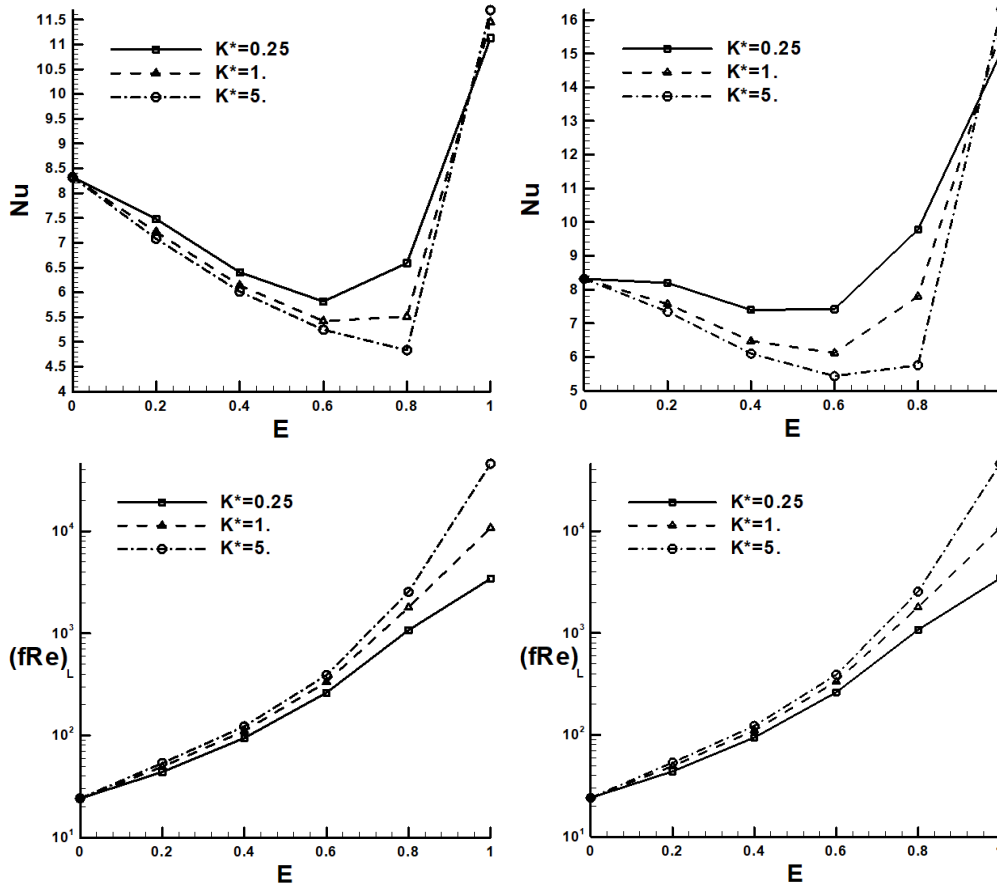


Figure 10. Effect of porous layer thickness E^* on the flow and heat transfer characteristics in the partially filled channel for different permeability ratios K^* (0.25, 1, 5) and different ratios of thermal conductivities R_k^* (1 and 0.1): $\theta = 0^\circ$, $Da = 10^{-3}$, $F = 0.1$: (a) Nusselt number for $R_k^* = 1$; (b) Nusselt number for $R_k^* = 0.1$; (c) friction coefficient for $R_k^* = 1$; and (d) friction coefficient for $R_k^* = 0.1$

4.2 Second Part: Combined Effects of Permeability, Anisotropy Orientation, and Porous Layer Thickness

4.2.1 Combined effect of permeability and anisotropy orientation angle on heat transfer enhancement

To study the combined impact of permeability (Da) and anisotropy orientation angle (θ) on heat transfer in a partially filled channel, we consider a fixed porous layer thickness ($E^* = 0.6$) (Figure 1). Predictions were made for Da values ranging from 10^{-4} to 10^{-1} , with $\theta = 0^\circ, 90^\circ$, and 180° , using $F = 0.1$ and $R_k^* = 1$, along with anisotropic parameters $K^* = 0.25$ and $K^* = 5$. The variations of the Nusselt number in terms of Da and anisotropy orientation angle of for these K^* values are shown in Figure 11. From Figure 11, we can observe:

(i) For $K^* = 0.25$, heat transfer by convection is minimal at $\theta = 90^\circ$ (highest vertical permeability) and maximal at $\theta = 0^\circ$ and 180° (insignificant vertical permeability). This trend reverses for $K^* = 5$.

(ii) The variation in Nusselt number is significant for higher Da values, while it is minimal for lower Da values, applicable to all tested Da values.

(iii) Heat transfer behavior in a channel partially filled with an anisotropic porous layer ($E^* = 0.6$) contrasts with that in a fully filled channel (see the study [21]).

Nevertheless, it is important to note that while optimizing heat transfer, the increased coefficient of friction due to the porous layer (and thus thickness E^*) must be considered. This factor is important for designing thermal systems,

such as heat exchangers. Consequently, the effect of the porous layer thickness should be further examined in the next subsection.

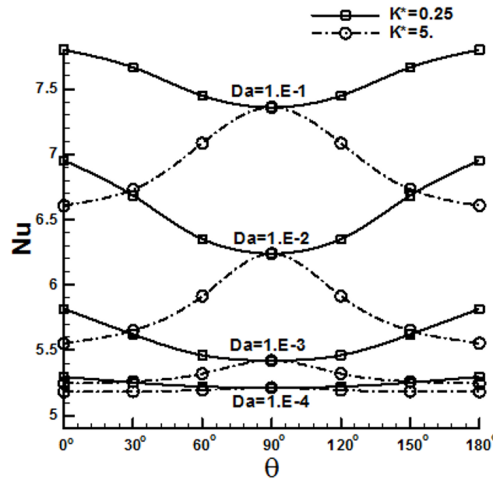


Figure 11. Variations of the Nusselt number along the partially filled channel ($E^* = 0.6$) in terms of Darcy number (Da) and the anisotropy orientation angle: Predictions were made for $K^* = 0.25$ and $K^* = 5$, with $F_o = 0.1$ and $R_k^* = 1$

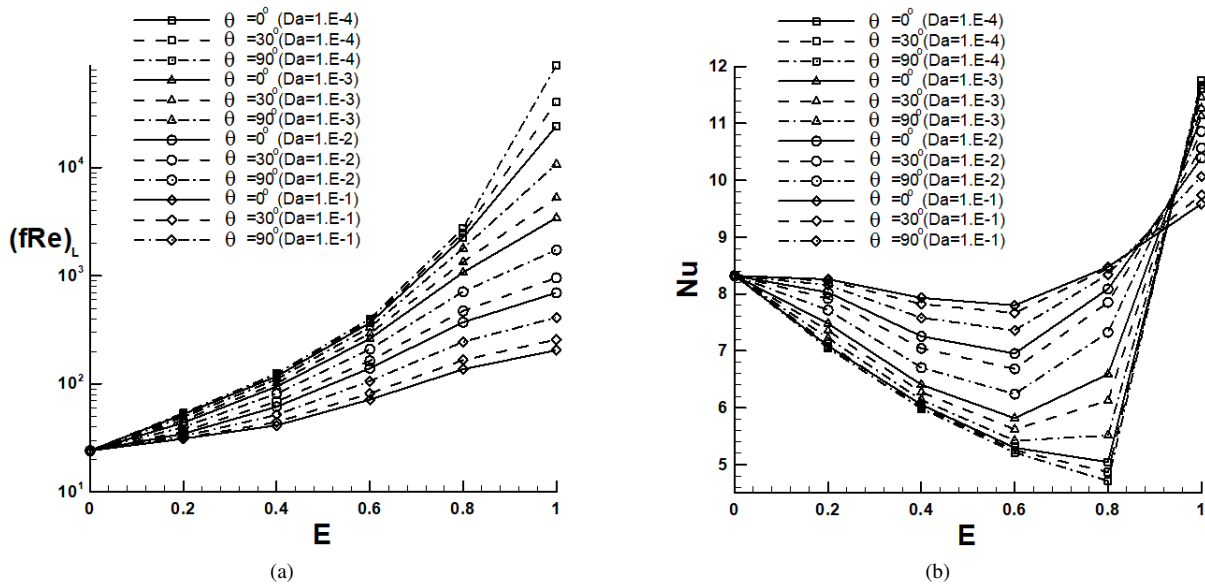


Figure 12. Combined effects of anisotropy orientation angle θ (0° , 30° , 90°), Darcy number Da (10^{-1} , 10^{-2} , 10^{-3} , 10^{-4}), and porous layer thickness E^* (between 0 and 1) on the flow and heat transfer characteristics in the fully developed region: $K^* = 0.25$, $F = 0.1$, and $R_k^* = 1$: (a) friction coefficient; and (b) Nusselt number

4.2.2 Combined effect of permeability, anisotropy orientation angle and layer thickness on fluid flow and heat transfer characteristics

To study the combined effect of permeability, anisotropy orientation angle, and porous layer thickness on fluid flow and heat transfer in a partially filled channel, we consider thickness varying from 0 to 1. Predictions are made for $K^* = 0.25$, with angles $\theta = 0^\circ$, 30° , and 90° , and permeability values between 10^{-4} and 10^{-1} , under conditions of $F = 0.1$ and $R_k^* = 1$. The variations in the coefficient of friction and the Nusselt number (in the developed region) with respect to Darcy number, thickness, and anisotropy orientation angle for $K^* = 0.25$ are shown in Figure 12a and Figure 12b, respectively. Examining these figures reveals the following findings:

(i) The coefficient varies with both the angle θ and thickness E^* . Increased thickness enhances the contact area between fluid and solid, while reduced permeability necessitates smaller pore sizes, leading to higher friction

resistance that exceeds the purely fluid case ($fRe = 24.1808$). This coefficient is inversely related to the Darcy number (see Figure 12a).

(ii) The Nusselt number decreases with increasing thickness until it reaches a minimum. Beyond this point, the trend reverses, resulting in values that surpass those of the purely fluid case (see Figure 12b).

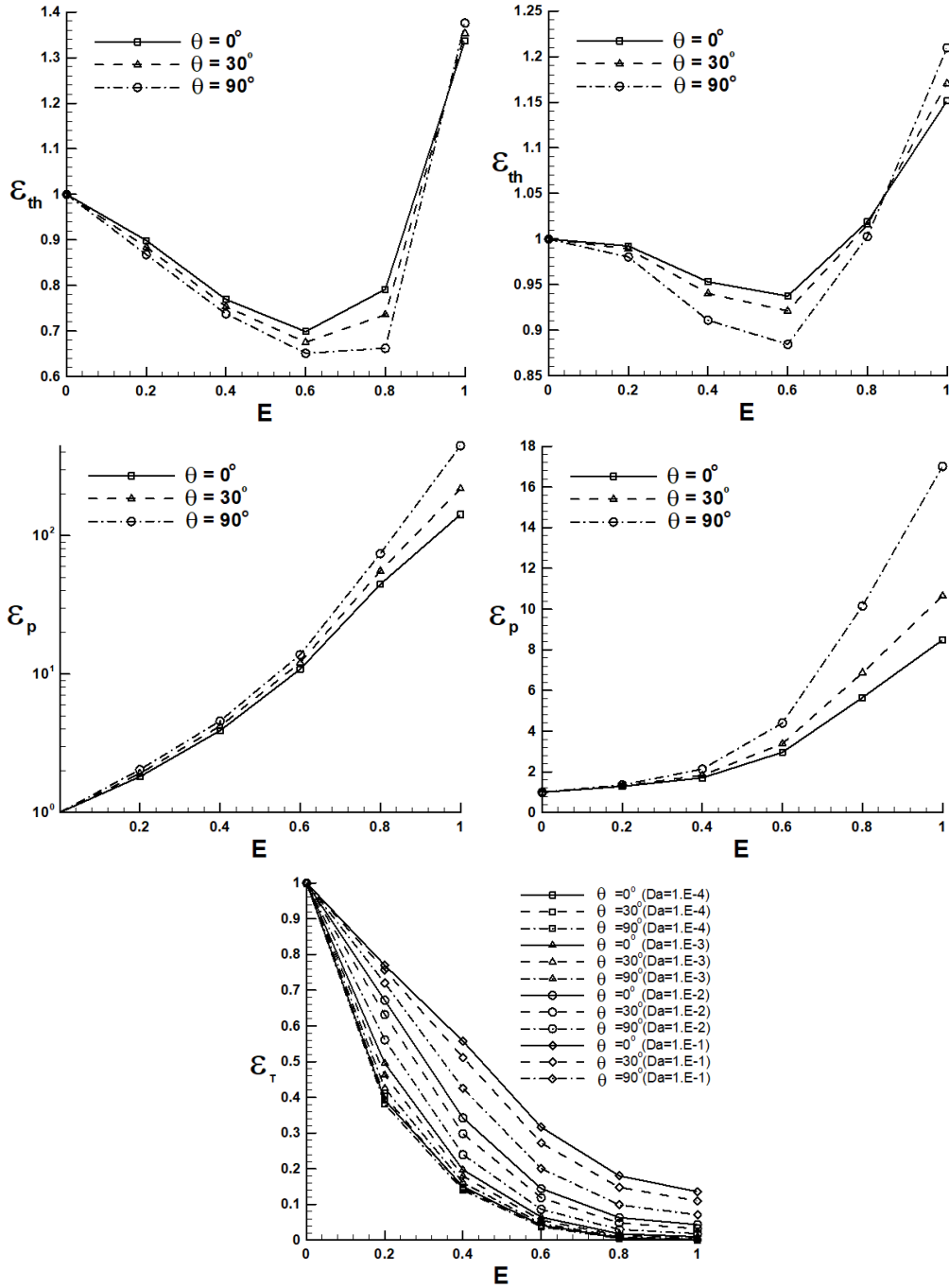


Figure 13. Effect of porous layer thickness E^* (between 0 and 1) on the heat transfer increment ratio, the friction coefficient increment ratio, and the evolutions of the overall thermohydraulic performance for different anisotropy orientation angles θ (0° , 30° , 90°): (a) heat transfer increment ratio for $Da = 10^{-3}$; (b) heat transfer increment ratio for $Da = 10^{-1}$; (c) friction coefficient increment ratio for $Da = 10^{-3}$; (d) friction coefficient increment ratio for 10^{-1} ; and (e) overall thermohydraulic performance for different Da ($10^{-1} - 10^{-4}$): $K^* = 0.25$, $F = 0.1$, $R_k^* = 1$

4.2.3 Prediction of heat transfer and friction coefficient increments ratios, and overall thermohydraulic performance ratio

Recall that to evaluate the effect of the porous layer on heat transfer, it is useful to normalize the Nusselt number Nu to that of a fully clear fluid channel, Nu_{cl} . Thus, we can express this as $\varepsilon_{th} = Nu/Nu_{cl}$. This quantity is known

as the heat transfer increment ratio, as described by Cekmer et al. [19]. For a clear fluid channel, the heat transfer increment ratio is equal to one, $\varepsilon_{th} = 1$. Similarly, the coefficient of friction increment ratio ε_p helps to evaluate the impact of the inserted porous layer on pressure drop. It is defined as the ratio of the friction coefficient fRe of the current channel (channel partially filled) to that of a channel with a pure fluid, fRe_{cl} (noting that $fRe_{cl} = 24.1808$); hence, $\varepsilon_p = fRe/fRe_{cl}$ [19]. Note that the ratio of ε_p to ε_{th} is typically referred to as the “overall thermohydraulic performance”. This ratio, $\varepsilon_T = \varepsilon_{th}/\varepsilon_p$, is commonly employed to compare the improvements in heat transfer and the associated pressure loss resulting from the insertion of the porous layer in the channel [19].

To study the improvement in heat transfer and the pressure drop caused by the insertion of the porous layer in a partially filled channel, we will consider the previously examined case in the above subsection. This time, we will analyze two cases of Darcy numbers ($Da = 10^{-3}$ and $Da = 10^{-1}$). The variations in the heat transfer increment ratio with respect to the thickness of the porous layer are presented in Figure 13a and Figure 13b. Additionally, the variations in the friction coefficient increment ratio as a function of the porous layer thickness are shown in Figure 13c and Figure 13d. Finally, Figure 13e illustrates the overall thermohydraulic performance ratio. Specifically, Figure 13e depicts the evolution of ε_T as a function of E^* for different values of Da and θ (with $K^* = 0.25$). An examination of Figure 13a to Figure 13e reveals the following insights:

First, Figure 13a and Figure 13b show that the use of a porous layer can reduce the heat transfer increment ratio to a minimal value ($\varepsilon_{th_{min}} < 1$), which depends on the thickness of the layer. After reaching this minimal value, the heat transfer increment ratio increases and exceeds unity ($\varepsilon_{th} > 1$), depending on both the Darcy number and the anisotropy orientation angle.

Similarly, Figure 13c and Figure 13d indicate that for Darcy numbers of 10^{-3} and 10^{-1} , the coefficient of friction increment ratio (ε_p) is greater than unity and increases with the thickness of the porous layer and the anisotropy orientation angle.

Finally, Figure 13e demonstrates that the increase in the coefficient of friction in the channel is greater than the increase in heat transfer. This is evident from the decreasing values of the overall thermohydraulic performance ratio ($\varepsilon_T < 1$). Additionally, Figure 13e reveals that the maximum heat transfer increment ratio occurs for a completely non-porous channel ($E^* = 0$). However, overall thermohydraulic performance is lower for $\theta = 90^\circ$ and higher for $\theta = 0^\circ$. The overall thermohydraulic performance also increases with an increasing Darcy number, and at low Darcy numbers, the anisotropy orientation angle has minimal effect on overall thermohydraulic performance.

5 Conclusion

From the parametric study on the characteristics of heat transfer and fluid flow in a channel partially filled with an anisotropic porous layer, we can draw the following conclusions:

5.1 Regarding Heat Transfer

- (1) The Forchheimer inertia coefficient influences heat transfer in isotropic porous media when $Da < 10^{-4}$.
- (2) Anisotropic parameters, including anisotropic permeability ratio, anisotropy orientation angle, and porous matrix thickness, significantly affect heat transfer:
 - Anisotropy orientation angle: For $\theta = 0^\circ$, the Nusselt number decreases with thickness to a minimum, then improves compared to clear fluid when $R_k^* = 1$.
 - Anisotropy permeability ratio: The highest Nusselt number occurs for $K^* < 1$ with thickness below the optimal level, enhancing heat transfer.
 - When thickness exceeds the optimal level, the highest Nusselt number is found for $K^* > 1$, especially at $R_k^* = 0.1$, surpassing values at $R_k^* = 1$.
- (3) Using a partially porous channel enhances the heat transfer coefficient for $R_k^* < 1$, particularly at $R_k^* = 0.1$ for low thermal conductivity media.

5.2 Regarding Fluid Flow

- (1) Anisotropic hydrodynamic parameters, including anisotropic permeability ratio, anisotropy orientation angle, and thickness of the porous matrix, significantly influence the flow field:
 - Friction Coefficient: The highest friction coefficient occurs for $K^* > 1$ (with $\theta = 0^\circ$) and $R_k^* < 1$ (with $\theta = 90^\circ$), indicating that using porous media with such anisotropic properties can help reduce the friction coefficient and pressure loss.
 - Thickness and Darcy Number: The coefficient of friction increases with the thickness of the porous layer, while its variation is inversely proportional to the Darcy number.
- (2) Utilizing a partially porous channel decreases the coefficient of friction when the ratio of thermal conductivities ratio is less than unity.

5.3 Regarding the Overall Thermohydraulic Performance

The overall thermohydraulic performance value for $K^* < 1$ decreases with increasing thickness, being lowest at $\theta = 90^\circ$ and highest at $\theta = 0^\circ$. However, it increases with Da . When Da is small, the performance is unaffected by the anisotropy orientation angle. This suggests the optimal choice of porous medium should have a permeability value (Da) not exceeding 0.1.

5.4 Suggestions for Heat Transfer Improvement

In order to improve the heat transfer, we can suggest (1) increasing the thickness of the porous layer in the channel until the Nusselt number exceeds its value in a channel entirely filled with fluid; this makes it possible to reduce the coefficient of friction if we compare it to that obtained for the totally porous case, (2) choosing porous media which have low thermal conductivities in order to reduce the ratio of thermal conductivities, and (3) the choice of the porous medium must be made taking into account the effects of the anisotropic permeability ratio and the anisotropy orientation angle, when the permeability in the direction of flow is less than that in the transverse direction.

5.5 Perspectives

The present numerical study clearly indicates that it is possible to intensively study the possibilities of increasing the heat transfer by modifying the values of the appropriate anisotropic hydrodynamic parameters of the porous layer. This study can be extended to deal with the influence of other parameters such as the positions of the porous layer in the channel in order to determine the effect of the position of the layer on the overall thermohydraulic performance; likewise, specific studies can be carried out to treat for example: the case of a thermally anisotropic porous layer, or that of a porous layer whose anisotropic hydrodynamic parameters are variable or the case of the presence of a non-local thermal equilibrium between the fluid and the layer. In addition, the present problem of forced convection in a channel partially filled with fluid saturated porous medium can also be modeled using other numerical tool such as the promising lattice Boltzmann method. This task represents our objective for future work.

Author Contributions

Conceptualization, S.B.A., R.K., and F.M.; methodology, S.B.A., R.K., and F.M.; software, S.B.A.; validation, S.B.A.; formal analysis, S.B.A., R.K., and F.M.; writing—original draft preparation, S.B.A., R.K., and F.M.; writing—review and editing, S.B.A., R.K., and F.M. All authors have read and agreed to the published version of the manuscript.

Data Availability

The data used to support the research findings are available from the corresponding author upon request.

Conflicts of Interest

The authors declare no conflicts of interest.

References

- [1] K. Vafai, *Handbook of Porous Media*, 2nd ed. Taylor and Francis Group, 2005.
- [2] D. A. Nield and A. Bejan, *Convection in Porous Media*. New York, USA: Springer, 1992.
- [3] M. Kaviany, *Principles of Heat Transfer in Porous Media*. New York, USA: Springer, 1995.
- [4] D. B. Ingham, A. Bejan, E. Mamut, and I. Pop, *Emerging Technologies and Techniques in Porous Media*. Dordrecht: Springer, 2004.
- [5] R. K. Shah and A. L. London, *Laminar Flow Forced Convection in Ducts: A Source Book for Compact Heat Exchanger Analytical Data*. New York: Academic Press, 1978.
- [6] A. Jamarani, M. Maerefat, N. F. Jouybari, and M. E. Nimvari, "Thermal performance evaluation of a double-tube heat exchanger partially filled with porous media under turbulent flow regime," *Transp. Porous Media*, vol. 120, pp. 449–471, 2017. <https://doi.org/10.1007/s11242-017-0933-x>
- [7] S. A. E. Sayed Ahmed, O. M. Mesalhy, and M. A. Abdelatif, "Flow and heat transfer enhancement in tube heat exchangers," *Heat Mass Transf.*, vol. 51, pp. 1607–1630, 2015. <https://doi.org/10.1007/s00231-015-1669-1>
- [8] S. Rashidi, J. A. Esfahani, and N. Karimi, "Porous materials in building energy technologies—A review of the applications, modelling and experiments," *Renew. Sust. Energ. Rev.*, vol. 91, pp. 229–247, 2018. <https://doi.org/10.1016/j.rser.2018.03.092>
- [9] P. Forooghi, M. Abkar, and M. Saffar-Aval, "Steady and unsteady heat transfer in a channel partially filled with porous media under thermal non-equilibrium condition," *Transp. Porous Media*, vol. 86, pp. 177–198, 2011. <https://doi.org/10.1007/s11242-010-9615-7>

- [10] W. K. Tien, R. H. Yeh, and J. C. Hsiao, "Numerical analysis of laminar flow and heat transfer in internally finned tubes," *Heat Transf. Eng.*, vol. 33, no. 11, pp. 957–971, 2012. <https://doi.org/10.1080/01457632.2012.654729>
- [11] R. Srijik, H. Brezet, and J. Vergeest, "Methods for conceptual thermal design," *Heat Transf. Eng.*, vol. 31, no. 6, pp. 433–448, 2010. <https://doi.org/10.1080/01457630903408318>
- [12] M. A. Yassin, M. H. Shedid, H. M. Abd El-Hameed, and A. Basheer, "Heat transfer augmentation for annular flow due to rotation of inner finned pipe," *Int. J. Therm. Sci.*, vol. 134, pp. 653–660, 2018. <https://doi.org/10.1016/j.ijthermalsci.2018.05.033>
- [13] B. Q. Zhao, A. Pantokratoras, T. G. Fang, and S. J. Liao, "Flow of a weakly conducting fluid in a channel filled with a Darcy–Brinkman–Forchheimer porous medium," *Transp. Porous Media*, vol. 85, pp. 131–142, 2010. <https://doi.org/10.1007/s11242-010-9550-7>
- [14] P. Wang, S. Yoon, Y. Yu, and Z. Shen, "Experimental study on the active enhancement mechanisms of heat and mass transfer in an absorption chiller (RP-1462)," *Sci. Technol. Built Environ.*, vol. 25, no. 1, pp. 58–68, 2019. <https://doi.org/10.1080/23744731.2018.1498668>
- [15] A. V. Kuznetsov, "Analytical investigation of the fluid flow in the interface region between a porous medium and a clear fluid in channels partially filled with a porous medium," *Appl. Sci. Res.*, vol. 56, pp. 53–67, 1996. <https://doi.org/10.1007/BF02282922>
- [16] A. V. Kuznetsov, "Study of forced convection in the presence of a liquid-porous-medium interface," *J. Eng. Phys. Thermophys.*, vol. 70, pp. 853–859, 1997. <https://doi.org/10.1007/s10891-997-0033-9>
- [17] A. V. Kuznetsov, "Analytical study of fluid flow and heat transfer during forced convection in a composite channel partly filled with a Brinkman–Forchheimer porous medium," *Flow Turbul. Combust.*, vol. 60, pp. 173–192, 1998. <https://doi.org/10.1023/A:1009998703180>
- [18] A. V. Kuznetsov, "Analytical investigation of forced convection from a flat plate enhanced by a porous substrate," *Acta Mech.*, vol. 137, pp. 211–223, 1999. <https://doi.org/10.1007/BF01179210>
- [19] O. Cekmer, M. Mobedi, B. Ozerdem, and I. Pop, "Fully developed forced convection in a parallel plate channel with a centered porous layer," *Transp. Porous Media*, vol. 93, pp. 179–201, 2012. <https://doi.org/10.1007/s11242-012-9951-x>
- [20] M. Maerefat, S. Y. Mahmoudi, and K. Mazaheri, "Numerical simulation of forced convection enhancement in a pipe by porous inserts," *Heat Transf. Eng.*, vol. 32, pp. 45–56, 2011. <https://doi.org/10.1080/01457631003732854>
- [21] G. Degan, S. Zohoun, and P. Vasseur, "Forced convection in horizontal porous channels with hydrodynamic anisotropy," *Int. J. Heat Mass Transf.*, vol. 45, pp. 3181–3188, 2002. [https://doi.org/10.1016/S0017-9310\(02\)0032-7](https://doi.org/10.1016/S0017-9310(02)0032-7)
- [22] G. Castinel and M. Combarous, "Critère d'apparition de la convection naturelle dans une couche poreuse anisotrope horizontale," *C. R. Seances Acad. Sci. Ser. B*, vol. 278, pp. 701–704, 1974.
- [23] G. Degan and P. Vasseur, "Aiding mixed convection through a vertical anisotropic porous channel with oblique principal axes," *Int. J. Eng. Sci.*, vol. 40, pp. 193–209, 2002. [https://doi.org/10.1016/S0020-7225\(01\)00012-X](https://doi.org/10.1016/S0020-7225(01)00012-X)
- [24] A. Nakayama, F. Kuwahara, T. Umemoto, and T. Hayashi, "Heat and fluid flow within an anisotropic porous medium," *J. Heat Transfer*, vol. 124, no. 4, pp. 746–753, 2002. <https://doi.org/10.1115/1.1481355>
- [25] L. E. Howle and J. G. Georgiadis, "Natural convection in porous media with anisotropic dispersive thermal conductivity," *Int. J. Heat Mass Transf.*, vol. 37, pp. 1081–1094, 1994. [https://doi.org/10.1016/0017-9310\(94\)90194-5](https://doi.org/10.1016/0017-9310(94)90194-5)
- [26] M. Karimi-Fard, M. C. Charrier-Mojtabi, and K. Vafai, "Non-darcian effects on double-diffusive convection within a porous medium," *Numer. Heat Transf. A*, vol. 31, pp. 837–852, 1997. <https://doi.org/10.1080/10407789708914067>
- [27] P. Bera, V. Eswaran, and P. Singh, "Numerical study of heat and mass transfer in an anisotropic porous enclosure due to constant heating and cooling," *Numer. Heat Transf. A*, vol. 34, pp. 887–905, 1998. <https://doi.org/10.1080/10407789808914021>
- [28] G. Degan, P. Vasseur, and E. Bilgen, "Convective heat transfer in a vertical anisotropic porous layer," *Int. J. Heat Mass Transf.*, vol. 38, no. 11, pp. 1975–1987, 1995. [https://doi.org/10.1016/0017-9310\(94\)00330-X](https://doi.org/10.1016/0017-9310(94)00330-X)
- [29] S. Kimura, A. Okajima, and T. Kiwata, "Natural convection heat transfer in an anisotropic porous cavity heated from side (2nd report, experiment using a Hele-Shaw cell)," *Heat Transf.*, vol. 31, no. 6, pp. 463–474, 2002. <https://doi.org/10.1002/htj.10046>
- [30] T. Aicher and H. Martin, "New correlations for mixed turbulent natural and forced convection heat transfer in vertical tubes," *Int. J. Heat Mass Transf.*, vol. 40, no. 15, pp. 3617–3626, 1997. [https://doi.org/10.1016/S0017-9310\(97\)00026-4](https://doi.org/10.1016/S0017-9310(97)00026-4)
- [31] S. V. Patankar, *Numerical Heat Transfer and Fluid Flow*. New York, NY: CRC Press, 1980.

- [32] F. M. White, *Viscous Fluid Flow*, 3rd ed. New York: McGraw-Hill, 2006.
- [33] I. Pop and D. B. Ingham, *Transport Phenomena in Porous Media II*, 1st ed. Oxford, UK: Pergamon, 2002.
- [34] J. C. Umavathi, J. P. Kumar, A. J. Chamkha, and I. Pop, "Mixed convection in a vertical porous channel," *Transp. Porous Media*, vol. 61, pp. 315–335, 2005. <https://doi.org/10.1007/s11242-005-0260-5>

Nomenclature

C_p	Heat capacity, J/kg · K
e_p	Thickness of the porous layer, m
f'	Coefficient of friction
f	Dimensionless coefficient of friction
$f(Re)_{2H}$	Product of the coefficient of friction by the Reynolds number
h	Local convective heat transfer coefficient, W/m ² · K
$2H$	Width of the entire channel ("double" characteristic length), m
k	Thermal conductivity, W/m · K
[K]	Anisotropic permeability tensor, m ²
K_1, K_2	Anisotropic permeability tensor components on the two main axes (x', y') of the porous medium, m ²
l	Length of channel, m
Nu	Nusselt number
Nu_{av}	Average Nusselt number along the channel
p'	Pressure, Pa
q_w	Heat flux per area unit, W/m ²
t'	Time, s
T'	Temperature, K
T'_e	Temperature at the channel inlet, K
\vec{V}'	Velocity vector, m/s
u', v'	Horizontal and vertical velocity components in the main axes (x', y'), respectively, m/s
(x', y')	Main axes of the system, m
(x'_r, y'_r)	Global coordinate system with rotation θ (rotated coordinate system), m

Greek symbols

ε	Porosity
θ	Anisotropy orientation angle (inclination between the main axes), degrees (°)
μ	Dynamic viscosity, Pa · s
ν	Kinematic viscosity ($\nu = \mu/\rho$), m ² /s
ρ	Density, kg/m ³

Superscripts/subscripts

'	Prime: superscript used to represent physical quantities (velocity, temperature, pressure, etc.)
av	Average
e	Inlet of the channel
eff	Effective (used for porous layer)
f	Fluid
p	Porous
w	Wall
r	Index used to represent rotation matrices relating velocity components in two coordinate systems (x'_r, y'_r) and (x', y')

Dimensionless quantities and numbers

Da	Darcy number ($Da = K/H^2$)
E^*	Dimensionless thickness of the porous layer, $E^* = e_p/H$
F	Forchheimer inertia coefficient
K^*	Anisotropic permeability ratio ($K^* = K_1/K_2$)
L^*	Aspect ratio of the channel ($L^* = l/H$)
Pr	Prandtl number ($Pr = \nu_f/\alpha_f$)
R_k^*	Ratio of the thermal conductivities ($R_k^* = k_{eff}/k_f$)
R_v^*	Ratio of the kinematic viscosities ($R_v^* = \nu_{eff}/\nu_f$)
Re	Reynolds number ($Re = u'_e H/\nu_f$)
$(Re)_{2H}$	Reynolds number based on $2H$ ($(Re)_{2H} = u'_e(2H)/\nu_f$)
ε_p	Friction coefficient increment ratio, $\varepsilon_p = fRe/(fRe)_{cl}$
ε_{th}	Heat transfer increment ratio, $\varepsilon_{th} = Nu/Nu_{cl}$
ε_T	Overall thermohydraulic performance, $\varepsilon_T = \varepsilon_{th}/\varepsilon_p$